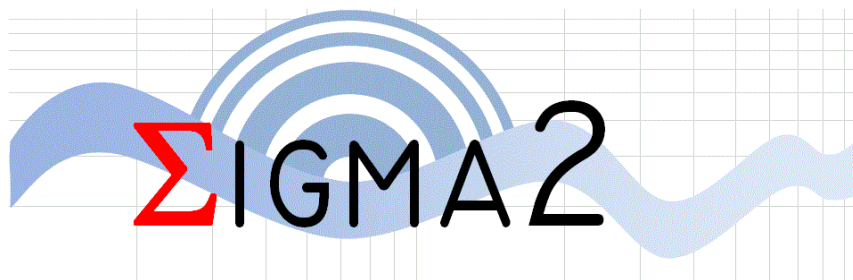# Ground motion model for reference rock sites

WORK PACKAGE 3 - GROUND MOTION

AUTHORS		REVIEW		APPROVAL	
Name	Date	Name	Date	Name	Date
Giovanni Lanzano Chiara Felicetta Francesca Pacor	2020/11/25	*J. Douglas*	2021/01/13	Emmanuel Viallet ***Public access*** ⊙ ***SIGMA-2 restricted*** ○	2021/12/12

Lanzano G., Felicetta C., Pacor F. - Metodology to identify reference rock sites - SIGMA2-2020-D3-047

Document history

DATE	VERSION	COMMENTS
YYYY/MM/DD	*0*	

INDEX

Executive summary

This document is the second-year report of the scientific activities in the framework of the collaboration between the EDF (Electricité DE France) company and the INGV (Istituto Nazionale di Geofisica e Vulcanologia) of Milan in the framework of SIGMA2 project (https://www.sigma-2.net), with the aim to improve the strategy for the reference rock sites identification and ground-motion modeling (GMM).

Starting from the results obtained last year for Central Italy, in this work we update the methodology for the identification of reference rock sites (hereinafter called Reference-Rock Identification Method, RRIM) and show an application for the whole Italian territory. The RRIM is based on two elements: 1) the identification of site parameters representing the reference site conditions and 2) the construction of the scoring scheme to classify candidate stations.

The set of proxies is composed by six parameters: three are related to the analysis of geophysical and seismological data (site term from residual analysis, resonance frequencies from Horizontal-to-Vertical spectral ratios, time-average shear-wave velocity in the first 30m); the remaining ones concern geomorphological and installation features (outcropping rocks or stiff soils, flat topography and absence of interaction with structures). Following the Decision Matrix Method (DDM), that is a qualitative technique used to rank the multi-dimensional alternatives of an option set, RRIM introduces a decision matrix consisting in a set of criteria, weighted in order of relevance, scored and summed to gain a total score.

We apply RRIM to a very large dataset, extracted from the last release of Italian Accelerometric Archive (ITACA v3.1), composed by more than 1600 stations. Given the large number of sites, the pre-selection of candidates is performed via residual analysis, selecting those with flat site response and amplitude similar or lower than the one for the generic rocks ($V_{S,30}$=800m/s). At the aim, we calibrated a GMM for the Fourier amplitudes spectrum (FAS), using the same functional form and dataset adopted for the reference Italian model, valid for acceleration response spectra (SA). Finally, to estimate the corrective factors from generic-to-reference rocks, we carry out a residual analysis on about 700 data recorded by the stations identified by RRIM.

The main results of this study are:

1. a set of coefficients for the prediction of 81 ordinates of the FAS for Joyner-Boore and rupture distances in the frequency interval 0.1-30Hz, consistent with those proposed by Lanzano et al. (2019a) for Spectral Accelerations (named ITA18);

2. a list of the reference rock sites in Italy among the recording stations available in the ITACA 3.1 database (http://itaca.mi.ingv.it ; D'Amico et al. 2020). The RRIM allowed us to identify 116 stations mainly installed along the Apennine chain, and in the areas of Hyblaean Mountains (Sicily), Gargano Promontory (Puglia) and Garda Lake (Lombardy). The associated mean $V_{S,30}$ is equal to 905m/s, if only measured values are considered. The list includes the majority of stations already identified in Central Italy (SIGMA2-2019-D3-027/1), based on a different dataset and reference GMM, confirming the robustness of the RRIM.

3. the period/frequency-dependent corrective terms for ITA18 generic-rock predictions to obtain the corresponding FAS and SA values at reference rock sites. The generic-to reference rock scaling has a significant effect at high frequencies, reducing, on average, the ground motion by up to a factor 1.7 at T = 0.1s/f =10Hz. The trend of the corrective terms resembles the inverse of the amplification factors from very hard rock to rock sites proposed by Van Houtte et al. (2011) for the host-to-target adjustment method (Campbell, 2003);

4. a preliminary model for the generic-to-reference rock corrective factors, parametrized in terms of $V_{S,30}$ and κ_0, the high-frequency decay parameter, introduced by Anderson and Hough, (1984). This model represents a meaningful addiction to the GMM for reference rock sites from 3Hz onwards and is able to fit the averaged reference rock spectra with κ_0 = 0.01s and $V_{S,30}$=900m/s.

Introduction

This deliverable describes the developments achieved for the proposal of a methodology for the identification of reference rock sites. Last year, in the deliverable SIGMA2-2019-D3-027/1, the methodology was applied to the Central Italy, using a large number of seismic records, composed of more than 450 stations, which led to the identification of 36 reference sites out of 133 candidates. The research is now extended to the whole of Italy, thus including different seismic contexts and geological formations, with the aim of generalizing the results obtained in a specific region.

Identifying a reference site via a set of proxies is a non-trivial matter. The common practice is to assume that sites where rocks or stiff soils outcrop and the time-average shear-wave velocity in the uppermost 30m ($V_{s,30}$) exceeds a given value represent an example of reference sites. However, the simple definition of reference rock sites based only on geological features and measurements of the shear-wave profiles, does not ensure the identification of sites whose amplification is expected to be negligible (Lanzano et al., 2020).

The methodology proposed to identify reference rock sites starts from the results obtained by Felicetta et al. (2018), that developed a procedure to recognize reference rock sites among the recording stations of the Italian ACcelerometric Archive (ITACA, http://itaca.mi.ingv.it; Luzi et al. 2008; Pacor et al. 2011) using six proxies, based on geological, topographical and geophysical parameters. Three proxies out of six are based on geophysical and seismological data, whereas the remaining three are based on geological and geomorphological features (outcropping rock, flat topography and absence of interaction with structures).

In the application to the Central Italy (Deliverable SIGMA2-2019-D3-027/1; Lanzano et al., 2020), in addition to updating the selected proxies, a mechanism derived from Decision Matrix Method (DDM) was proposed to weigh the different parameters and obtain a ranking of candidate sites as references. This mechanism is based on: i) a hierarchical index (HI), variable from 0.5 to 2, to take into account the capability of the proxy to represent the seismic response of the stations and ii) a proxy weight (PW), variable from 0 to 1, to take into account the presence/absence and the quality of the information relative to the proxy. By the combination of hierarchical indexes and weights, an overall score was assigned and the reference sites were recognized as those that exceed a given threshold.

At the end, the set of proxies adopted in the Central Italy study was composed by six site-parameters: three are related to the analysis of geophysical and seismological data (site term from residual analysis, resonance frequencies from Horizontal-to-Vertical spectral ratios, $V_{S,30}$); the remaining ones concern geomorphological and installation features (outcropping rocks or stiff soils, flat topography and absence of interaction with structures).

Several comparisons were performed to evaluate the impact of the introduction of the 36 identified reference rock-stations into GMM calibration: their use slightly affects the low frequency median ground-motion while leads to a significant reduction at high-frequency that is up to 40% at T=0.1s: the predicted levels are even lower than the median values predicted by the national model (ITA18, Lanzano et al., 2019), for sites with $V_{S,30}$ equal to 1500 m/s. This result suggests that the seismic motion level for the reference sites does not simply scale with the $V_{S,30}$, but also depends on additional site parameters.

The study of reference sites has several objectives: (i) to establish a procedure for their identification; (ii) to assess the impact on the ground-motion; and (iii) to define the scaling with respect to generic rock. In this deliverable, we test the applicability of the procedure developed for Central Italy identifying the reference stations throughout Italy. Then, instead of calibrating a new GMM for reference sites, we estimate the frequency dependent corrective factors to scale the ground-motion predicted for generic rock to the reference level. At this aim, we consider the ITA18 model recently calibrated for acceleration response spectra of shallow crustal earthquakes in Italy, in which the reference ground-motion level is estimated for $V_{S,30}$=800m/s. Moreover, to extend our results to the Fourier domain, we calibrate a new model for Fourier Amplitude Spectra (FAS), using the same dataset of the ITA18 model.

This deliverable is organized as follows: in the first chapter, we describe the ITA18 FAS model; consistent with the ITA18 model, which will be used both to calculate the site residuals in the Fourier domain. The second chapter is dedicated to the preliminary selection of candidate stations to be a reference site, using a larger dataset of Italian records, extracted by ITACA. The selection is carried out by means a cluster analysis of the site residuals, evaluated with respect to the ITA18 predictions in FAS and response spectra. The collection of the site proxies and the building of the weighting scheme is described in chapter 3, while the ranking of the candidate stations is reported in chapter 4. Finally, in chapter 5, the generic-to-reference rock scaling factors are calibrated, via residual analysis.

ITA18 FAS model

The dataset for GMM calibration is the same as Lanzano et al. (2019a), in order to make the FAS model consistent with ITA18 for SA (named ITA18-SA). The records were selected from Engineering Strong Motion (ESM) flat-file (Lanzano et al. 2019b), according to the following criteria:
- Earthquakes of active shallow crustal regions in Italy (focal depth lower than 30km);
- Minimum moment magnitude set to 3.5;
- Joyner-Boore or rupture distance less than 200 km;
- Post-2009 events with a magnitude less than 5.0 are characterized by revised metadata and number of records higher than 10. Several aftershocks of major seismic sequence in Italy are disregarded, in order to have, as much as possible, a homogeneous distribution of events along the Italian territory;
- Only stations with surface instruments and with low or no interactions with nearby structures are included.

The records of twelve worldwide events with magnitude larger than 6.1, having a source geometry defined by specific literature studies, were also included. The moment magnitudes were assigned to the events following this hierarchy: i) European-Mediterranean Earthquake Catalogue (EMEC; Grünthal and Wahlström 2012); ii) literature studies; iii) Regional Centroid Moment Tensor (Pondrelli and Salimbeni 2015) and Centroid Moment Tensor (Ekström et al., 2012); iv) Time Domain Moment Tensor (Scognamiglio et al. 2009). The geometries of the fault ruptures are defined for the events with magnitude larger than 5.5. For smaller magnitude events, we consider point-like sources since the differences between the epicentral and Joyner-Boore distances as well as between the hypocentral and rupture distances can be neglected.

The final selection includes 5607 records, relative to 146 earthquakes and 1657 stations. About 486 stations are characterized by measured $V_{S,30}$ which corresponds to 1560 records (about 1/4 of the dataset). In case of missing $V_{S,30}$, they have been inferred from slope (Wald and Allen, 2007). We prefer to use the slope as a proxy for $V_{S,30}$ instead of geology, since, applying the available tools (Di Capua et al. 2011; Forte et al. 2019), you can only define a characteristic site category (e.g. according to EC8 site classification) or an average $V_{S,30}$, while using topography you can adjust $V_{S,30}$ continuously as a function of slope. However, we use surface geology as a check, verifying that the $V_{S,30}$ from slope would allow us to classify the site in the same subsoil category that would be obtained from geology.

Figure 1a shows the locations of the selected events in Italy: earthquakes with magnitude larger than 5.5 are mainly located in Central Italy and the predominant style of faulting is normal, as the seismicity of the Italian peninsula is dominated by the tectonic extension along the Apennine chain. Figure 1b shows the magnitude-distance distribution (Joyner-Boore distance) of the regional versus worldwide records: since such events could be not representative of the regional attenuation or stress drop of Italian events, the percentage of worldwide records is small (14% of the total number of records).

(a)   (b)
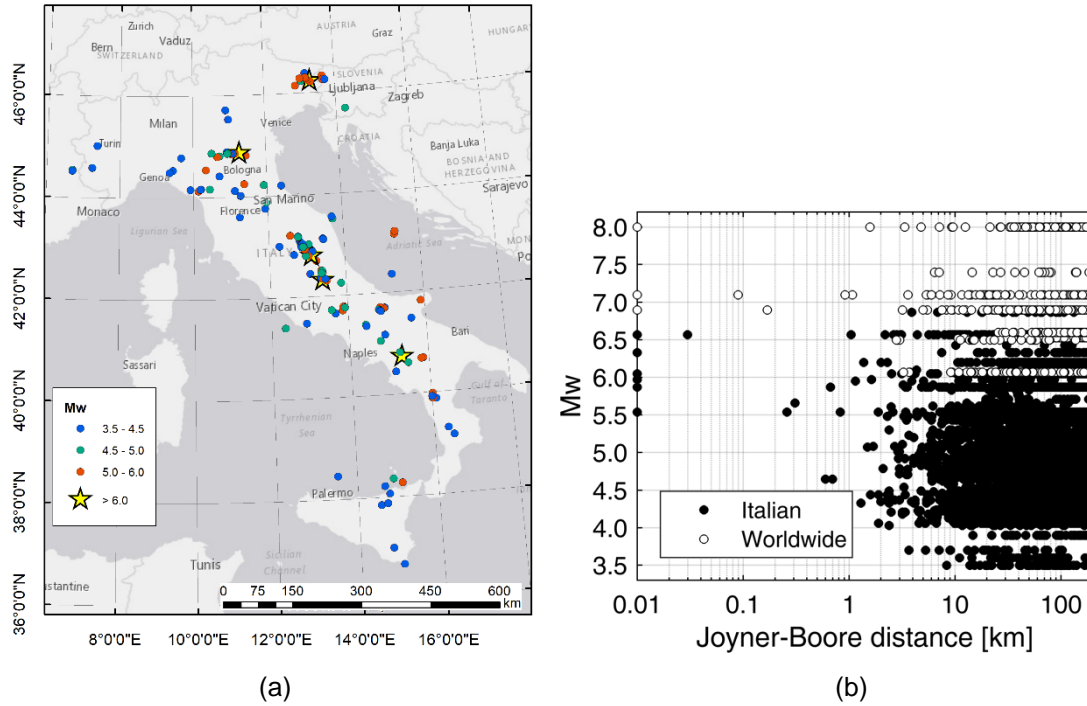
Figure 1. a) spatial distribution of the events in Italy employed for ITA18 FAS calibration (from Lanzano et al. 2019c); b) magnitude-distance distribution of the calibration dataset (from Lanzano et al. 2019a).

We adopt the same functional form used for SA calibration:

$$\log_{10} Y = a + F_M(M_W,\text{SOF}) + F_D(M_W,R) + F_S(V_{S,30}) + \sigma \qquad [1]$$

$$F_M(M_W,\text{SOF}) = f_j \text{SOF}_j + \begin{cases} b_1(M_W - M_h) & \text{where } M_W \leq M_h \\ b_2(M_W - M_h) & \text{where } M_W > M_h \end{cases} \qquad [2]$$

$$F_D(M_W,R) = [c_1(M_W - M_{\text{ref}}) + c_2]\log_{10}\sqrt{R^2 + h^2} + c_3\sqrt{R^2 + h^2} \qquad [3]$$

$$F_S(V_{S,30}) = k\log_{10}\left(\frac{V_0}{800}\right) \quad \begin{array}{l} V_0 = V_{S,30} \quad \text{for } V_{S,30} \leq 1500\,m/s \\ V_0 = 1500\,m/s \quad \text{for } V_{S,30} > 1500\,m/s \end{array} \qquad [4]$$

$$\sigma = \sqrt{\tau^2 + \varphi_{S2S}^2 + \varphi_0^2} \qquad [5]$$

Y is the observed intensity measure (*IM*), i.e. the 81 ordinates of FAS in the frequency range 0.1–30Hz, calculated using the Konno & Ohmachi (1998) smoothing function (*b*=40). The prediction is valid for the geometric mean of the two horizontal components. Since the processing is manual, high- and low- pass filter corner frequencies may differ. As a result, the number of records varies with periods (Figure 2): 100% of the data is considered in the interval 1-10Hz; the calibration dataset is reduced by about 30% at f=0.1Hz and about 10% at 30Hz.
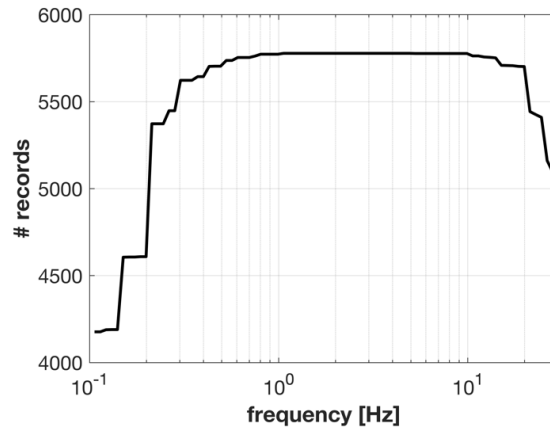
Figure 2. Number of FAS records versus frequency

We derived two different sets of coefficients for Joyner-Boore ($R=R_{JB}$) and rupture ($R=R_{rup}$) distances. The explanatory variables are: the moment magnitude (M_W), the source-to-site distance (R), the V_{S30}, and the styles of faulting (SOF_j), which are dummy variables, introduced to specify strike-slip ($j=1$), reverse ($j=2$), and normal ($j=3$) fault types. The hinge magnitude M_h and the reference magnitude M_{ref} are set to 6.0 and 5.0, respectively. The pseudo-depth (h) is set to 6.5km and 2.0km for the R_{JB} and R_{rup} models, respectively.

The coefficients a, b_1, b_2, c_1, c_2, c_3, k and f_j (f_1 for strike-slip, f_2 for thrust fault, and f_3 for normal fault) are derived by a second step mixed-effect linear regression (Bates et al. 2015). The random-effects are applied to stations and events, in order to estimate the partially non-ergodic sigma according to Al Atik et al (2010), where τ and ϕ_{S2S} represent between-event and site-to-site variability, respectively, and σ_0 is the standard deviation of the event- and site- corrected residuals. The coefficients and the standard deviations are available in the Appendix I.

In order to confirm the goodness of the results, several plots are available in Appendix II, including the graphs of the residual components as a function of the explanatory variables and the model predictions and observations as a function of distance. Figure 3a compares the τ, ϕ_{S2S} and σ_0 standard deviations of the FAS model for R_{JB} and R_{rup}; Figure 3b shows the total standard deviation σ of the FAS model in R_{JB}, compared to that obtained for ITA18-SA model, computed according to Eq [5].

(a)   (b)

Figure 3. Standard deviations of ITA18-FAS models vs frequency. Left: R_{JB} vs. R_{rup}; right: FAS (R_{JB}) vs. SA (R_{JB}).

The between-event standard deviation (τ) exhibits values in the interval 0.12-0.27 log10 units, with lowest values between 0.5 and 4Hz. Event- and site- corrected standard deviations (σ_0) are almost const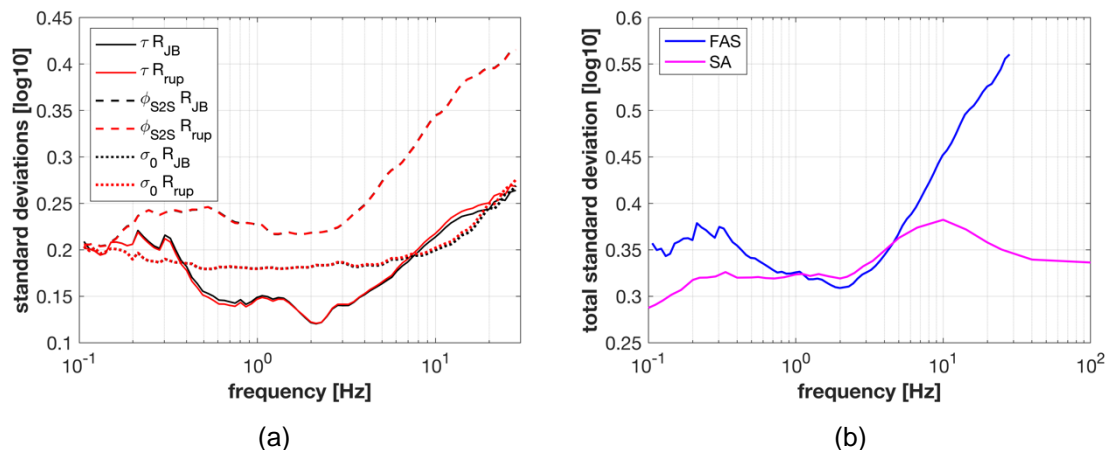ant around 0.19 in a wide frequency range (0.1-10Hz) and, afterwards, increase as the frequency increases (up to 0.27). The largest contribution of total sigma is due to site-to-site variability (ϕ_{S2S}) especially at high frequencies, moving from about 0.24 log10 units at 3Hz to over 0.4 at 30Hz. The main cause of the larger ϕ_{S2S} variability of FAS model w.r.t. SA is related to the differences between FAS and the corresponding SA: the response spectral accelerations at high frequencies are controlled a much wider range of frequencies than Fourier amplitudes (Bora et al., 2016); as a consequence, narrow-band site effects at short periods have a larger impact on Fourier amplitudes whereas for response spectral accelerations they are smoothed out. Other studies have shown that if you use the same functional for model calibration, the high frequency variability increases for FAS compared to SA (Bindi et al., 2019a; 2019b). No significant differences are found between the R_{JB} and R_{rup} FAS models. As a result, the minimum total variability is at 2Hz (about 0.31), while maximum value is about 0.56 at 30Hz. Such values are remarkably higher than those found for SA calibration at highest frequencies, while they are very similar in the interval 1-5Hz. The large values of the standard deviation components at high frequency is quite common in the FAS model calibration, such as the model proposed by Bindi et al. (2019) for Central Italy, which adopted a functional form very similar to Eq.[1], leading to a total standard deviation of $0.61\log_{10}$ units at 25Hz. Bora et al. (2015), instead, proposed a more complex equation, including the dependence on stress drop and high frequency attenuation parameter, resulting in $0.3\log_{10}$ units at same frequency.

Table 1 provides some statistical tests for the coefficients of few representative Fourier amplitudes (f=0.1, 2 and 28Hz). The statistical significance of the predictors is tested through the *p-value* (Wasserstein and Lazar, 2016). A low *p-value* (< 0.05) indicates that the null hypothesis can be rejected. In other words, a predictor that has a low *p-value* is likely to be a meaningful addition to the model because changes in the predictor's value are related to changes in the response variable. Concerning the goodness of fit, we compute the standard error associated with each coefficient.

Table 1. Statistical tests on calibration coefficients of the FAS model. SS: strike-slip; TF: reverse fault.

	Coefficient value			Standard error			p-Value		
	0.1Hz	2Hz	28Hz	0.1Hz	2Hz	28Hz	0.1Hz	2Hz	28Hz
a	0.689	2.664	2.820	0.067	0.048	0.091	≪ 0.05	0	≪ 0.05
b_1	1.341	0.492	0.309	0.042	0.026	0.051	≪ 0.05	≪ 0.05	≪ 0.05
b_2	0.964	0.153	0.348	0.080	0.048	0.101	≪ 0.05	< 0.05	< 0.05
c_1	0.042	0.160	0.044	0.014	0.011	0.019	< 0.05	≪ 0.05	< 0.05
c_2	-0.712	-1.345	-2.591	0.034	0.030	0.051	≪ 0.05	0	0
c_3	-9.05E-05	-7.86E-04	1.78E-03	2.29E-04	1.92E-04	3.29E-04	0.692	≪ 0.05	≪ 0.05
k	-0.340	-0.653	-0.020	0.036	0.033	0.063	≪ 0.05	≪ 0.05	0.744
$f_1(SS)$	0.047	0.050	0.101	0.054	0.029	0.062	0.390	0.078	0.104
$f_2(TF)$	0.066	0.003	0.030	0.050	0.028	0.061	0.187	0.914	0.627

As for the SA model, the coefficients of style of faulting correction, f_1 and f_2, exhibit higher *p-values*, showing that these terms are not a meaningful addition to the model (Bommer et al. 2003). We can report *p-values* > 0.05 for the c_3 coefficient at low frequencies and the k coefficient at high frequencies. The first remark is still consistent with the SA model, for which the anelastic attenuation term has been removed at long periods because it is not significant with respect to geometric attenuation.

As regards the coefficient k, Figure 4 also reports the $V_{S,30}$ scaling at two FAS ordinates, corresponding to low and high frequencies. At high frequencies (around 15Hz) even positive scaling is achieved, albeit with rather low values, which causes a moderate increase of amplification with $V_{S,30}$, but more evidence that this explanatory variable is not able to describe the site effects at such frequencies.

(a)   (b)
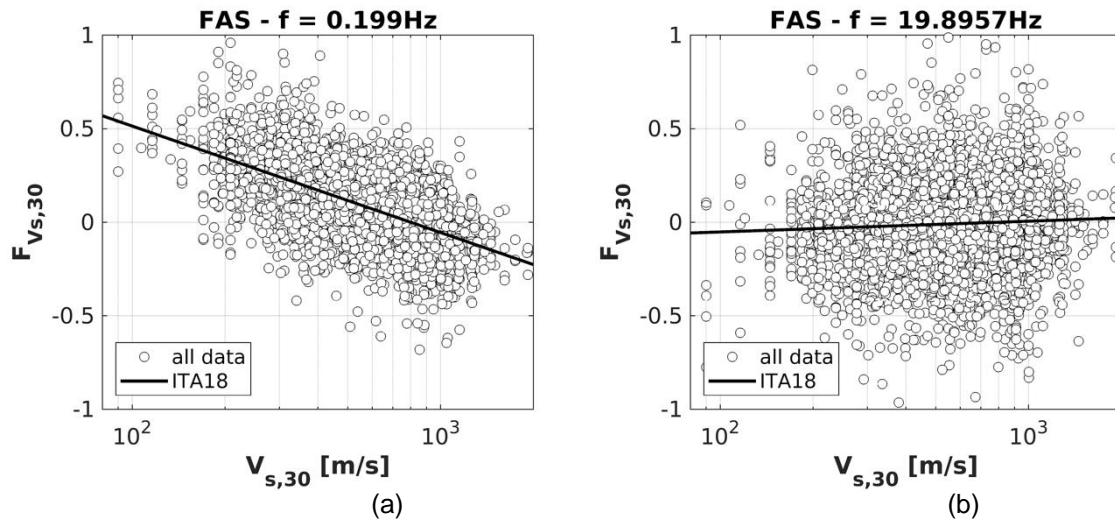
Figure 4. Site term (Eq. [4]) as a function of $V_{S,30}$ against the residuals corrected for source and distance terms: a) f = 0.2Hz and b) f = 20Hz.

Figure 5 compares the $V_{S,30}$ scaling, i.e. the values of coefficient k against frequency, and the associate p-values for FAS and SA models. The calibration coefficients are very similar in large range of frequencies, from 0.2 to 6Hz. *P-values* of FAS become higher than 0.05 where the differences between the k values of SA and FAS are larger (f>10Hz).

(a)   (b)
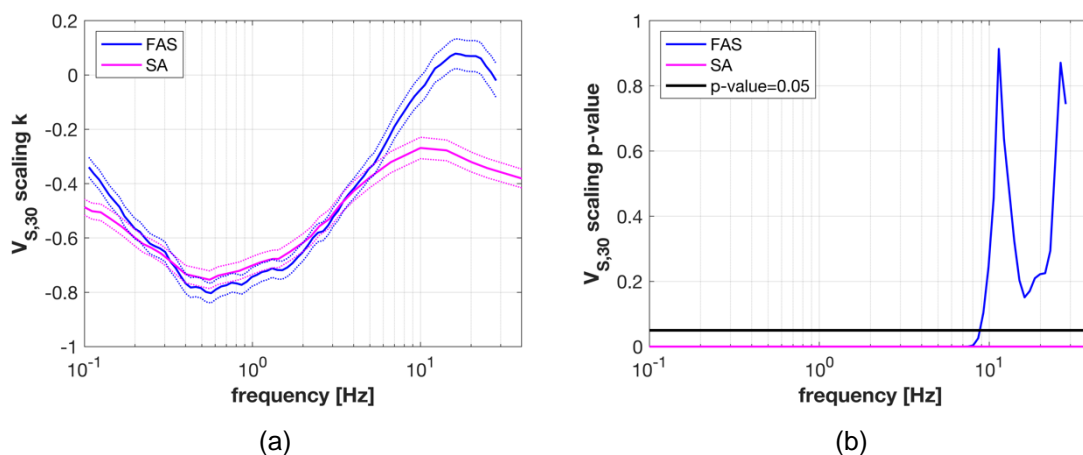
Figure 5. a) calibration coefficient k as a function of frequency for FAS and SA ITA18 models; b) p-values of k as a function of frequency for FAS and SA.

Selection of the candidate sites

For the selection of the candidate stations to be reference rock sites, we prefer to employ a "station-based" dataset, rather than an "event-based" dataset like that used for the calibration of the ITA18 FAS

model, with the final aim to have a more robust estimation of the systematic station residual terms. For such reason, we use the waveforms collection of the last release of ITACA (ITalian ACcelerometric Archive v.3.1; http://itaca.mi.ingv.it ; D'Amico et al. 2020), which represents the most complete collection of records of moderate-to-severe earthquakes (M>3.0) occurred in Italy in the period 1972 – 2019 from permanent and temporary accelerometric stations. The records are processed uniformly with the procedure described in Puglia et al. (2018). All data contained in ITACA are yearly updated and subjected to a review process of the event and station metadata. The latter are fully traceable including all the references of each metadata. The authoritative sources and the criteria for the attribution of the metadata are explained in Luzi et al. (2016) and Lanzano et al. (2019b) for the related database ESM (Engineering Strong Motion Database; https://esm.mi.ingv.it), but they are also valid for ITACA.

In the last ten years, great efforts have been spent to characterize the seismic stations in Italy (Felicetta et al., 2017): in the framework of the agreement (2010-2020) between the Italian Civil Protection and INGV, a task was devoted to increase the level of completeness of site information of the permanent recording stations contained in the ITACA database, and to store the results, also improving the tools for their dissemination. In this context, resonance frequencies from noise and earthquake records have been estimated, by means a standard procedure. Moreover, geological maps at different scales have been produced and invasive and non-invasive techniques have been applied to measure the S-wave velocity profile at least down to 30m. To date, about 30% of Italian stations have a detailed characterization, which allows the estimation of three site parameters: the resonance frequency, the measurement of $V_{S,30}$ and the surface geology (>1:10,000). Concerning the temporary stations, the site characterization is poor, however several data can be recovered by the microzonation studies and by the analysis of continuous seismic records, especially in the areas struck by the seismic sequences. This amount of information is exploited in this study to classify the stations of the dataset and, in the next chapter, ranking the candidate sites.

Starting from the initial collection of ITACA, the final set of data for residual analysis is retrieved adopting the following selection criteria:

- epicentral distance lower than 220km;
- exclusion of volcanic and subduction events;
- event shallower than 30km;
- exclusion of the borehole and station installed on the building elevation floors.

We also include the records of the networks of the neighboring countries, such as France, Switzerland, Slovenia, Albania and Montenegro to have a more robust estimation of the residual event term. Furthermore, we add the records of several velocimetric stations especially in southern Italy, collected in the framework of the HYPSTHER project (D'Amico et al. 2018), removing the records affected by instrument saturation.

The number of records of such dataset is 32600 for 1756 earthquakes and 1716 stations. The event and stations spatial distribution is shown in Figure 6: most of the events (Figure 6a) have epicenter along the Apennine chain, in the Eastern Sicily, in Friuli, and around the Garda Lake (between Lombardy and Veneto). The distribution of the stations (Figure 6b) across the Italian territory is very dense, except some areas where the seismicity is lower, such as Sardinia Island, the coastal area of Tuscany, the Salento peninsula and some areas in the Piedmont. However, such collection of recording sites represents almost all the geologic environments present in Italy.

Figure 7 shows the distribution of the station in function of the $V_{S,30}$ and the number of records. Like for the ITA18 dataset, about 22% of the stations (374) are characterized by measured $V_{S,30}$ and, in case of missing data, they have been inferred from slope, according to the procedure by Wald and Allen (2007). The majority of the stations have $V_{S,30}$ values in the interval 200-800m/s (about 70%), and the most populated range is 400-600m/s composed of about 500 recording stations. Very few stations are characterized by $V_{S,30}>1200$m/s, which reflects the features of the outcropping geology in Italy, mainly composed of stiff soils and soft rocks. A large number of stations recorded more than 5 records (Figure

7b), corresponding to about 60%, with not negligible amount of recording sites with more than 30 records (about 300 stations).
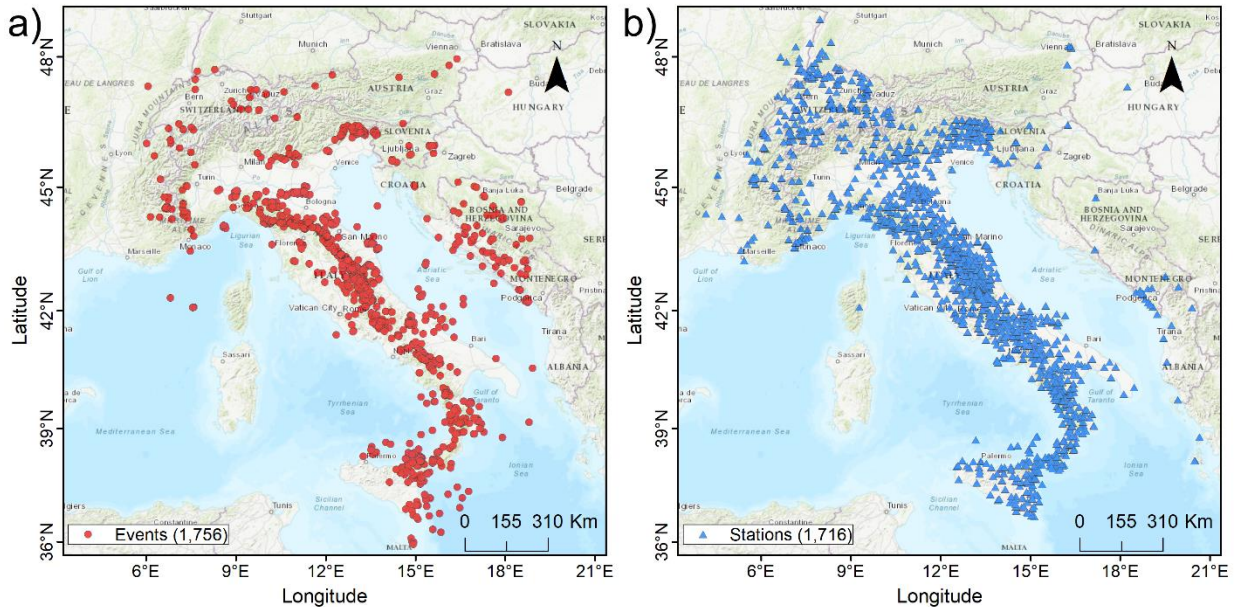
Figure 6. Spatial distribution of epicenters of the events (a) and recording stations (b) included in the ITACA dataset.
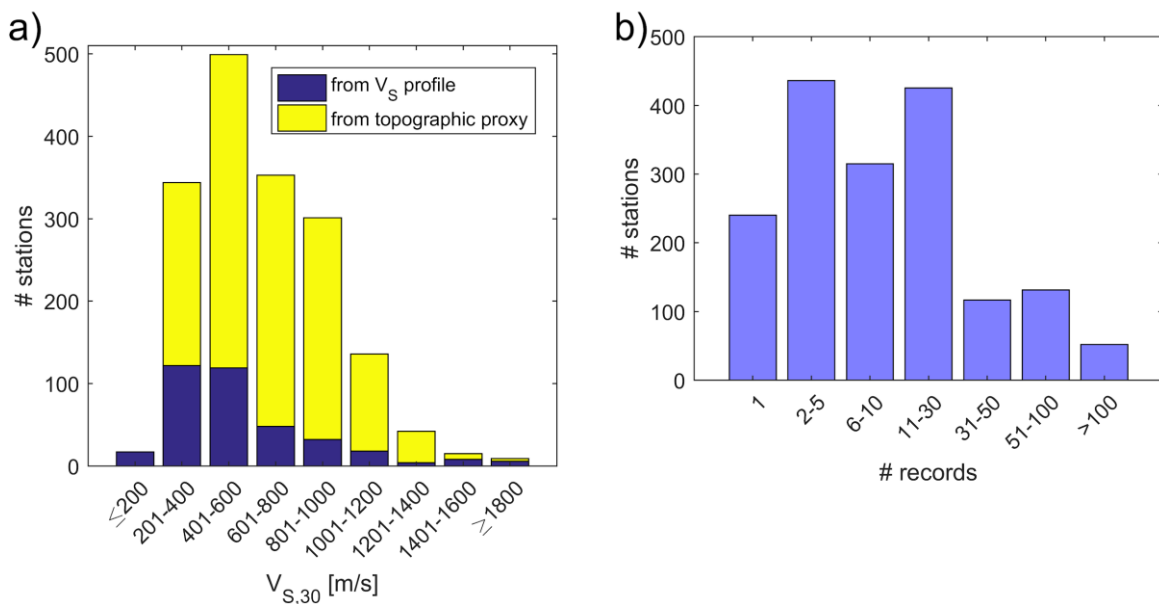
Figure 7. Distribution of recording station as a function of a) $V_{S,30}$ and b) number of records.

In order to pre-select the candidate reference rock stations, we compute the residuals both for SA and FAS ordinates. The reference models are ITA18-SA for response spectra and ITA18-FAS, calibrated in §1 for Fourier spectra. Following the Al Atik et al. (2010) scheme, the residuals are decomposed in between-event, site-to-site and event- and site- corrected components and computed by means of the application of the random-effect model (Stafford, 2014).

For the purpose of this study, following the procedure described in the Deliverable SIGMA2-2019-D3-027/1, we compute the site-to-site term with respect to reference site condition of ITA18, i.e. $V_{S,30}$=800m/s. In this way, the site-to-site term, named $\delta S2S_{800}$, represents an empirical amplification

function of the station, with respect to the generic rock prediction. We expect that the candidates for reference rock sites exhibit negative or almost zero values of $\delta S2S_{800}$ at all periods, since the ITA18 includes both reference sites and stations affected by amplifications.

Our strategy to identify the candidate reference rock sites is to perform a cluster analysis on the $\delta S2S_{800}$ curves (as a function of period) with the aim of detecting the sites belonging to the class with the lowest values and flat trend. Recently, this approach to interpret the seismic behavior of the recording stations on the basis of the automatic aggregation of the site-to-site curves is becoming popular recently, like in the work of Kotha et al. (2018), applied over the Japanese Kik-Net dataset.

Considering the procedure to estimate the residual terms (Stafford, 2014), the $\delta S2S_{800}$, used for cluster analysis, are calculated on, at least, 5 records. As a result, the number of investigated stations is 1028. For the clustering in FAS, the frequency interval, considered in the analysis, is 0.2-20Hz, while for SA is 0.01(PGA)-5s.

Among several techniques for data aggregation available in literature, we use the *k-means* clustering (David and Vassilvitskii, 2007) to partition the observations of the *n*-by-*p* matrix into k clusters, where *n* is the number of sites and *p* is the number of parameters. The main advantage of this method is that it converges very quickly, but the number of the cluster must be assigned a-priori. The analysis is carried out on the amplification factors ($e^{\delta S2S}$), through the *k-means* function, available in the Matlab Package 2019b. After some trials, we set the number of k = 8, even though it is not the optimal number of clusters (Tibshirani et al. 2001) but in this way, the clusters of stations with ground-motion level lower or similar to the generic rock prediction of ITA18 ($V_{S,30}$=800m/s) are clearly represented and distinguished. Figure 8 reports the mean amplification curves $e^{\delta S2S}$ as a function of period for the 8 clusters for FAS and SA.
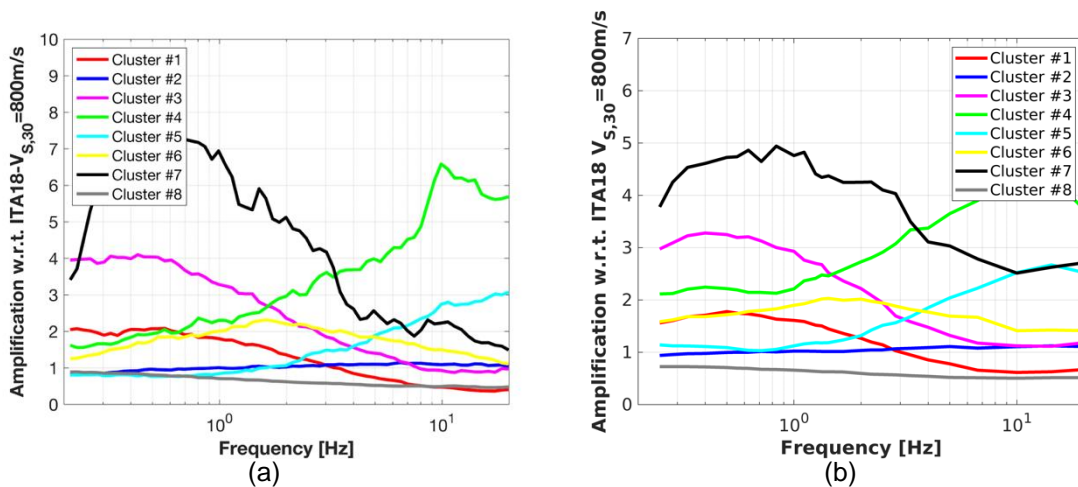
Figure 8. Results of cluster analysis: a) FAS; b) SA.

Both for SA and FAS, two clusters of the candidate reference rock sites are recognizable: both have flat trend but different level of amplification (with respect to the mean prediction of rock sites of the reference ground motion model), i.e. less than 1 (de-amplification) for the former (cluster #8, hereinafter set A) and equal to 1 (no amplification) for the latter (cluster #2, hereinafter set B). The main relevant differences between the FAS and SA clusters are relative to the most amplified clusters: as an example, cluster #7 in FAS exhibits higher amplification (around 7.5) at low frequencies with respect to the corresponding cluster in SA (lower than 5). Same finding is observed at high frequencies for cluster #4 in FAS (maximum amplification of 6.5 around 10Hz) and SA (amplification about 4.5). The total number of pre-selected stations in SA is 492, while in FAS it is 478. The two subsets have 453 in common, corresponding to 92% and 95% of the total in SA and FAS, respectively. The pre-selected stations in SA, but not in FAS, are 43, most of which (58%) belong to the cluster of stations with moderate high frequency amplification. We also verified that, starting from both the pre-selection in SA and FAS, the stations selected as reference sites (according

to the procedure illustrated in the next section) were the same, since they are all part of the 453 stations in common.

The selected clusters for FAS are showed in Figure 9: set A ($e^{\delta S2S}$ of cluster #8) contains stations characterized by a de-amplification and a quite flat trend at all periods; while the set B (cluster #2) exhibits, on average, zero amplification at all periods, i.e. it includes sites having a mean ground motion response very similar to those predicted by ITA18 for $V_{S,30}$=800m/s.
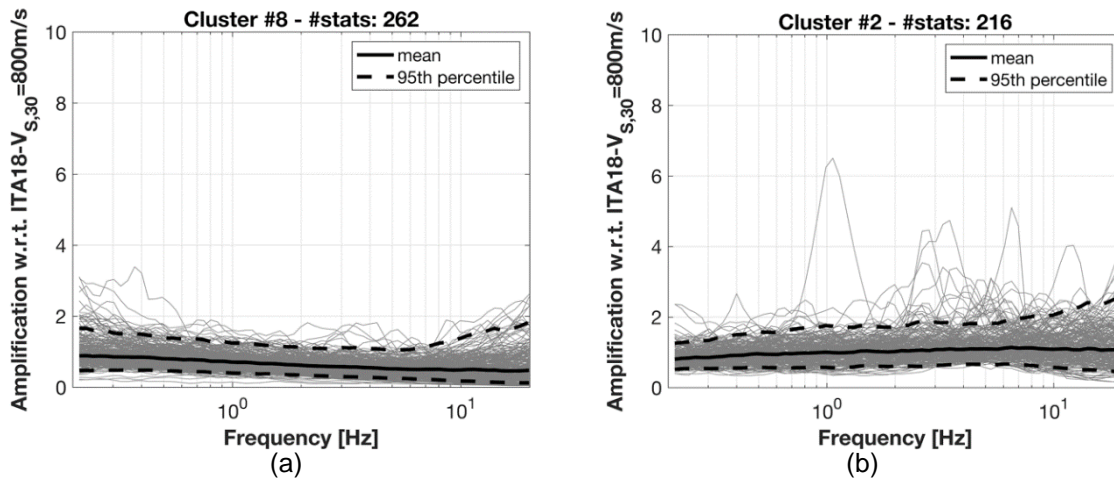
Figure 9. Amplification ($e^{\delta S2S}$) vs frequency: a) set A; b) set B.

Looking at the amplification curves, there are a few stations in set B with high amplifications at some narrow frequency bands. Possible causes are: i) the number of clusters could be not optimal; as an example, in the work of Lanzano et al. (2020), the cluster analysis was performed with 9 classes (instead of the 8 presented here) and showed less outliers (see Figure 5 of Lanzano et al. 2020) than the ones obtained for Italy; ii) compared to the SA, the FAS residuals are less smoothed and single peaks can be frequently observed in some station, even if the general trend of the $e^{\delta S2S}$ term resembles the mean curve of the stations in the cluster. However, this is not a very critical issue, since the subsequent weight assignment process (next section) ensures that these stations are then excluded from the final selection. Indeed, any site can be subjected to the identification process through RRIM; this pre-selection step was necessary due to the high number of starting stations of our analysis.

On the opposite, even if the station had a sufficient number of recordings, the flat and de-amplified trend of $\delta S2S_{800}$ (and an associated small variability), the only combination of these conditions does not guarantee that the site can be considered as a good reference site. As an example, we report the case of the TRN1 station (http://itaca.mi.ingv.it/ItacaNet_31/#/station/IT/TRN1) of the RAN network (netcode: IT) installed in the municipality of Terni in the Umbria region (Central Italy). The $\delta S2S_{800}$ and H/V both show a flat and not amplified trend and are estimated with an adequate number of recordings (174 for $\delta S2S_{800}$ and 79 for H/V): this would suggest that TRN1 is a good candidate as a reference site. The analysis of the outcropping geology and the installation conditions of the station says the opposite, since the station is located in an alluvial deposit and is installed in an underground garage. Probably, the confinement effect of the ground on the side of the garage is the cause of the flat and not amplified trend of the amplification function.

In the following analyses, we prefer to perform the station pre-selection based on the results of FAS analysis, as they provide an empirical estimate of the amplitudes of the site transfer function.

The number of the pre-selected stations of set B is 216 and that of set A is 262, for a total number of 478 candidate stations, corresponding to the 46% of the total number (478 vs. 1028). 433 stations are

installed on the Italian territory and belong to Italian seismic networks. The remaining are part of international networks operated by various providers and located along the borders with Italy. In the following section, we consider only the Italian stations due to the availability of metadata deriving from detailed seismic site characterization.

Proxies and weighting schema

This chapter is focused on the description of the RRIM. The approach has been developed in the Deliverable SIGMA2-2019-D3-027/1 and updated in Lanzano et al., 2020 (submitted). It derived from the decision-matrix method (DMM, Pugh, 1981), that is a qualitative technique used to rank the multi-dimensional alternatives of an option set. To our aim, we adopt a weighted decision matrix consisting in a set of criteria, weighted in order of relevance, scored and summed to gain a total score which can be ranked.

In order to handle the relevance, the data quality and the possible lacking of these indicators, the RRIM is based on a weighting scheme given by the combination of two values: the hierarchical index (HI) and the proxy weight (PW). The former expresses the importance of the proxy in representing the site effect, the latter evaluates the extent to which the single proxy is fulfilled.

By means the application of the weighting scheme to the stations belonging set A and B, we award a final ranking of the candidates to be reference sites. The proposed proxies and the acceptance criteria are listed in Table 2, while the assigned weights and scores are listed in Table 3.

Table 2. List of the proxies used to identify reference rock stations.

#	PROXY	ACCEPTANCE CRITERION
1	Site-to-Site term of the horizontal components (δS2S)	negative or close to 0 on the entire period range
2	Housing (HOU)	absent or limited interaction with structures (free-field condition)
3	Topographic condition (TOP)	flat or smooth topographic surface
4	Surface geology (GEO)	rock or stiff conditions from geological/lithological map
5	Average shear wave velocity in the first 30 m (VS30) measured or inferred from proxies	$V_{S,30} > 600$ m/s
6	Horizontal-to-Vertical spectral ratio (H/V) of Fourier spectra of noise measurements (HVNSR) or coda-waves (HVSR-C) or S-waves (HVSR-S) or acceleration response spectra of earthquake records (HVRS)	flat or moderately broad-band curve

Following the previous study (SIGMA2-2019-D3-027/1), in addition of the horizontal site-to-site terms proxy (δS2S), used to pre-select the possible reference stations, we consider further five proxies based on seismological data (H/V), and on geophysical, geological, geomorphological and installation features (VS30, GEO, TOP, HOU). These proxies (or their combination) were already satisfactorily used to verify that there are no site-effects at rock stations (Felicetta et al., 2018; Luzi et al.; 2019; Priolo et al.; 2019). Indeed, these site parameters can be easily obtained in contexts of medium-high seismicity, where datasets rich in recordings are available, many stations are installed, geological maps are available throughout the entire territory and many sites are characterized by geophysical tests.

The assignment to the weight according to the proxy values (PW, listed in Table 3), is based on the following general rules:

- If the criterion is met, the weight is set equal to 1;
- If the proxy value does not fulfill the requirement, the weight is set equal to 0;
- When the criteria are partially met, the weights may range from 0.25 to 0.75.

Differently from the previous study (SIGMA2-2019-D3-027/1), where the lack of information was weighed 0.5, in this work, the weight is set equal to 0 if no data are available for the proxy.

Moreover, since the selected proxies have different capability to represent the seismic response, the HI is variable from 0.5 to 2 (Table 3). We assume that the most important indicators for site-effect characterization, with HI=2, are the surface geology (GEO), the VS30 and the HV from Fourier spectra, which are also indicated by recent results of the task devoted to the site effects in the SERA project (2017-2020, D7.2 Best practice for site characterization). The HOU and TOP proxies are considered less relevant for the purpose and HI is set equal to 0.5.

The score assigned to each proxy is given by the product between HI and PW. The complete fulfillment of the criteria listed in Table 3 defines the ideal reference rock site and corresponds to a total score of 8.

Table 3. Hierarchical index and weight values assigned to the proxies. $PW_0(V_{S,30})$ function is reported in Eq.[6].

Proxy	Hierarchical Index (HI)	Criterion		Proxy Weight (PW)
δS2S	1	cluster A within the 95% confidence interval*		1
		cluster A beyond the 95% confidence interval*		0.75
		cluster B within the 95% confidence interval*		0.75
		cluster B beyond the 95% confidence interval*		0.5
HOU	0.5	Free-field condition		1
		Electrical transformation cabin		0.75
VS30	2	Measured from geophysical in-situ tests		$1 * PW_0(V_{S,30})$ [Eq.6]
		Inferred from topographic proxy		$0.5 * PW_0(V_{S,30})$ [Eq. 6]
GEO	2	EC8-A (scale-map ≥ 1:10,000)		1
		EC8-A (scale-map < 1:10,000)		0.75
		EC8-B (scale-map ≥ 1:10,000)		0.5
		EC8-B (scale-map < 1:10,000)		0.25
TOP	0.5	slope ≤ 15°		1
		15° < slope ≤ 30°		0.5
H/V	2	Flat (amplitude < $2\sqrt{2}$)	HVNSR	1
			HVSR-C	1
			HVSR-S	0.5
			HVRS	0.5
		Broad-band (amplitude > $2\sqrt{2}$)	HVNSR	0.5
			HVSR-C	0.5
			HVSR-S	0.25
			HVRS	0.25

In the following, we provide a short description of the selected proxies and the associated acceptance criteria:

- **δS2S** is used to pre-select the possible reference rock stations since it is considered a proxy of the seismic response of the station (Al Atik et al. 2010), with the caveat that the amplification levels may be dependent on the reference sites adopted in the GMM calibration. The HI is set to 1 and the PW is assigned as a function of the cluster membership, attributing different values at clusters A and B and evaluating if the stations are or not within the 95% confidence interval of each cluster (Table 3).

- **HOU** is introduced to remove stations with possible dynamic interaction effects since many studies show that records of stations located inside or close to buildings may be affected by the

vibrations of the structure as well as by soil-structure interaction phenomena (Gallipoli et al., 2004; Stewart et al., 1999). The building proximity has been checked for the candidate stations. Following Abrahamson et al. (1991), we compute the minimum distance from the adjacent structure, based on the predominant vibration period of the structure NTC18 (Italian seismic code, 2018), that depend on the construction material and structure type. If the station does not respect the minimum distance or it is installed close to large dams (such as MSC station close to Campotosto dam in Central Italy) PW is set equal to 0. Moreover, in Italy, several stations belonging to the RAN network are located in electrical transformation cabins (Gorini et al., 2010), that affect the recordings at specific frequencies, usually larger than 5Hz (Ditommaso et al., 2010). For this reason, PW = 0.75 for sites installed inside electrical cabins or small buildings and PW = 1 for free-field stations.

- **GEO** is assigned on the base of geological or lithological maps (available at different scales) used to classify the station according to the lithological description of EC8 categories. The criterion is fully met when the station is installed on rock or other rock-like geological formation (EC8-A), as inferred from maps: PW=1 or 0.75 if map scale is greater or smaller than 1:10,000, respectively. For stations located on stiff soil (EC8-B) PW=0.5 or 0.25 if map scale is greater and lower than 1:10,000.

- **TOP** is introduced to exclude sites with possible amplifications due to particular topographic settings (Massa et al., 2014; Paolucci 2002). PW=1 if the site is located on either a flat surface or isolated slope and relief with average ground inclination from the horizontal plane less than 15°, following the prescriptions of some National building codes (AFPS95; CS.LL.PP-NTC18 2018). The weight is assumed to be zero if the slope is greater than 30°.

- **VS30** is the most common parameter used to recognize soils with similar response sites. Similarly, to NEHRP site classification (BSSC, 2003), we distinguish between hard and very hard rock sites, assigning different weights. With respect to the previous works (Lanzano et al., 2020), we recognized that weighting this parameters with a step function may be excessively penalizing for Vs30 values close to the threshold (e.g. $V_{S,30}$ around 750 m/s), considering the uncertainty related to the shear wave velocity profile estimation (Régnier et al., 2016). Our proposal is to adopt a piecewise linear function PW_0:

$$
PW_0(V_{S,30}) = \begin{cases} 0 & for\ V_{S,30} \leq 600m/s \\ 0.75 \cdot \frac{(V_{S,30}-600)}{(750-600)} & for\ 600 \leq V_{S,30} \leq 750m/s \\ 1 - \left[\frac{(1-0.75)}{(1500-750)} \cdot (1500-V_{S,30})\right] & for\ 750 \leq V_{S,30} \leq 1500m/s \\ 1 & for\ V_{S,30} \geq 1500m/s \end{cases} \quad [6]
$$

The final weight PW is dependent on how $V_{S,30}$ has been estimated:

$$
PW(V_{S,30}) = \alpha \cdot PW_0(V_{S,30}) \quad [7]
$$

where α=1 for $V_{S,30}$ measured from geophysical tests and α=0.5 in the case of $V_{S,30}$ inferred from empirical correlations. In the PW_0 function we reduce the threshold to 600 m/s, corresponding to one of the values proposed by Boore & Joyner (1997) for generic rocks.

- **H/V** curves are used to detect the fundamental resonance frequency of the site. We consider the H/V curves obtained from in-situ noise measurements (HVNSR; Nakamura, 1989; Bonnefoy-Claudet et al., 2008 and references listed therein) and, when they are not available, we evaluate the proxy based on earthquake records using FAS (Lermo and Chavez-Garcia, 1993; Puglia et al., 2011) of coda-waves (HVSR-C), or S-waves (HVSR-S) and 5% damped acceleration elastic response spectra (HVRS; Puglia et al., 2011; Felicetta et al., 2018; Hassani et al., 2019). Differently from the previous study (SIGMA2-2019-D3-027/1), in order to reduce

the number of criteria and avoid redundancy, we decided to include HVRS analysis as the last alternative if both HVNSR and HVSR are missing. Consequently, PW is assigned combining the type of estimate (HVNRS, HVSR-C, HVSR-S and HVRS) and the H/V curve shape (flat or broadband). HVSR-C curves are generally similar to HVNSR (Puglia et al., 2011; Stehly et al., 2006). HVSR-S are comparable to HVSR-C but the variability is generally higher, especially when directional effects are present or records from strong events at short epicentral distance are included (Puglia et al., 2011). Moreover, recent studies (Puglia et al., 2011; Felicetta et al., 2018; Hassani et al., 2019) showed that, in case of clear resonance frequencies, the outcomes from HVNSR and HVRS agree.

Station ranking

The overall scoring relative to each stations is given by the weighted sum of the scores assigned at each proxy as follows:

$$S = \sum HI_i * PW_i \; where \; i = 1, \dots, 6 \hspace{3cm} [8]$$

We assume that a station is a reference site if it reaches a minimum score of 4.75 out of 8 (Table 3). Adopting this threshold, almost 60% of the required criteria are met. In order to give a statistical meaning to the choice of the threshold, we compute the moments of the distribution of scores of all investigated stations: the median is 3.75, while the 84th percentile is 5.25. The adopted threshold corresponds to the 75th percentile of the score distribution.

After the application of the weighting scheme, we recognize 116 reference rock stations: 81 out of 236 of *cluster A* and 35 out of 197 of *cluster B.* The maximum score obtained by the candidate stations is 7.53, none reach the maximum awardable score (8) since the $V_{S,30}$. value greater than 1500 m/s is not represented in the Italian dataset. The selected stations are listed in Appendix III. As an example, in Table 4 we list the reference stations belonging to set A having the final score ≥ 6.5. Compared to the results of Lanzano et al (2020) for central Italy, the stations that were missed in the new selection are only 5: the stations ATVA and CAFR are not included in the analysis dataset because they have few records in ITACA; the three stations MZ102, SNAL and TRIV are not included in the pre-selection, since their $\delta S2S_A$ functions exhibit moderate amplifications.

Figure 10 shows the geographical distribution of the identified reference rock sites: these are mainly installed along the Apennine chain, and in the areas of Hyblaean Mountains (Sicily), Gargano Promontory (Puglia) and Garda Lake (Lombardy).

Table 4. Extract of the Appendix III: list of the cluster A stations with "Final score" ≥ 6.5. For each station, the table reports: network code (NET CODE); station code (STA CODE); weight for cluster #1 (δS2S score); housing/proximity condition (HOU); housing score (HOU score); scale of the geological/lithological/litothecnical map (GEO scale); EC8 subsoil classification from surface geology (EC8 GEO); weight for the geological proxy (GEO score); slope value (TOP); topographic weight (TOP score); $V_{S,30}$ value (VS30); $V_{S,30}$ estimation method (VS30 method); VS30 weight (VS30 score); shape of H/V curve (HV); H/V analysis (HV type); weight for the H/V proxy (HV score); number of available proxies (Av proxies). FF = free-field condition; CAB = Electrical transformation cabin; NO-FF = no free-field condition; F = flat curve; BB = broadband curve; P = picked curve; Meas = measured by geophysical test; Topog = inferred from topographic proxy.

NET CODE	STA CODE	δS2S score	HOU	HOU score	GEO scale	EC8 GEO	GEO score	TOP	TOP score	VS30 [m/s]	VS30 method	VS30 score	HV	HV type	HV score	Av. proxies	Final score
IT	MND	1	FF	0.5	10000	A	2	1.0	0.5	800	Meas	0.77	F	HVNSR	2	6	7.53
IT	PPL1	1	FF	0.5	10000	A	2	0.6	0.5	775	Meas	0.76	F	HVNSR	2	6	7.52
IT	SDG	0.75	FF	0.5	10000	A	2	0.8	0.5	800	Meas	0.77	F	HVNSR	2	6	7.28
IT	MNF	1	NO-FF	0	10000	A	2	16.4	0.25	1060	Meas	0.85	F	HVNSR	2	6	6.96
IT	BBN	0.75	FF	0.5	100000	A	1.5	9.5	0.5	1000	Meas	0.83	F	HVNSR	2	6	6.92
IT	SBC	1	FF	0.5	10000	A	2	10.9	0.5	1298	Meas	0.93	F	HVSR-S	1	6	6.87
IT	MZZ	1	FF	0.5	10000	A	2	9.3	0.5	794	Topog	0.76	F	HVNSR	2	6	6.76
IT	MVB	1	FF	0.5	5000	B	1	3.6	0.5	1046	Meas	0.85	F	HVNSR	2	6	6.70
IV	ATVO	1	FF	0.5	10000	B	1	8.6	0.5	1033	Meas	0.84	F	HVNSR	2	6	6.69
IT	SCN	1	FF	0.5	5000	A	2	10.4	0.5	839	Meas	0.78	BB	HVNSR	1	6	6.56
IT	LSP	0.75	FF	0.5	10000	A	2	12.8	0.5	886	Topog	0.80	F	HVNSR	2	6	6.55
IV	ATLO	1	FF	0.5	10000	B	1	3.3	0.5	767	Meas	0.76	F	HVNSR	2	6	6.51
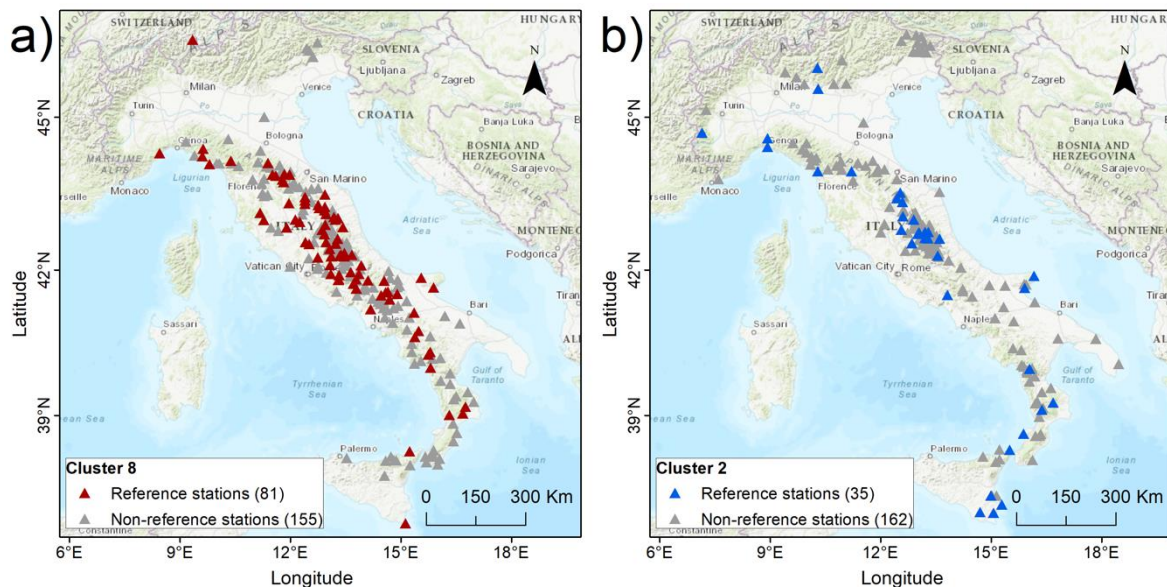
Figure 10. Geographical distribution of the reference stations selected from cluster A/#8 (a) and cluster B/#2 (b).

Figure 11 shows the distribution of the 116 reference rock-sites in terms of EC8 class inferred from surface geology, $V_{S,30}$ values, slope range, and shape of H/V curves. As expected, the majority of the candidates are located on rock (EC8$_{GEO}$-A) or stiff soil (EC8$_{GEO}$-B) conditions with flat topography (slope ≤ 15°) and the estimated H/V curves are flat (F). Few stations classified as EC8-C on the base of surface geology are installed on alluvial deposits with thicknesses of a few meters (IT.SDM, IT.BCN, IT.DCM); other analyses should be carried out to investigate in more detail the geomorphological contexts of these sites.

82% of the candidate stations has $V_{S,30}$ values greater than 750 m/s (lower limit of the norms), while 87% greater than 600 m/s (lower limit according to Boore and Joyner, 1997, and this study); for about

one third of the stations, the $V_{S,30}$ is estimated from the V_s profile (Figure 12) and the mean value is about 900 m/s; if both measured and inferred $V_{S,30}$ values are considered, the mean decreases to about 850 m/s. The profile of the V_s with depth estimated by Boore and Joyner (1997) for North America and Poggi et al. (2011) for Switzerland have been added to Figure 12 for comparison. The average of the reference sites is very similar to the model derived from Poggi et al. (2011) and is correctly included in the variability range of Boore & Joyner (1997), closer to the lower target of the generic rocks.

About 53% of the stations of set A and B that does not reach the threshold value are characterized by peaked H/V curves and 80% are classified in EC8-B and EC8-C soil categories, according to the outcropping geology. Finally, only 1% of the excluded stations have the $V_{S,30}$ values obtained from geophysical measurements larger than 750 m/s.
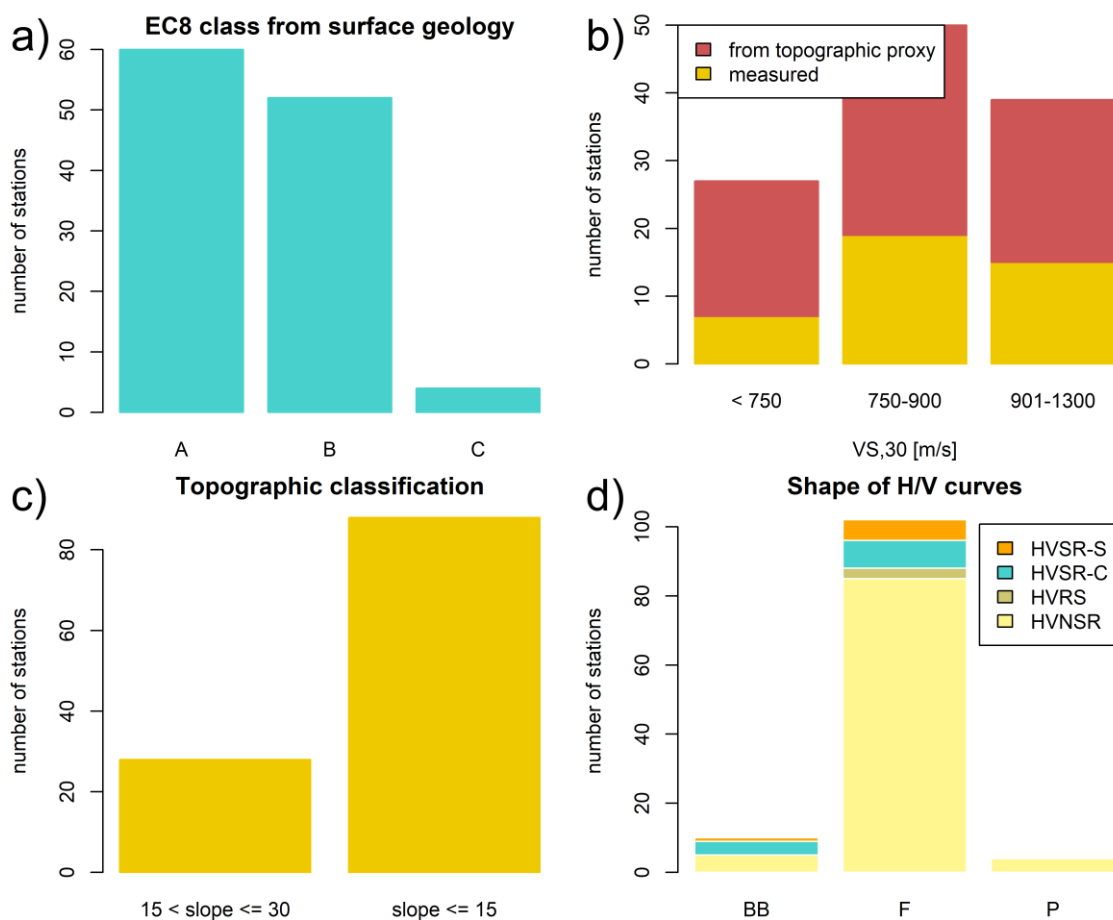
Figure 11. Distribution of the selected reference rock-sites in terms of: a) EC8 class inferred from surface geology (GEO proxy); b) $V_{S,30}$ as function of type (measured or inferred from topographic proxy); c) slope range (TOP proxy); d) shape of H/V curves colored as function of the analysis type (HVNSR in yellow, HVSR-C in teal, HVSR-S in orange; HVRS light brown).
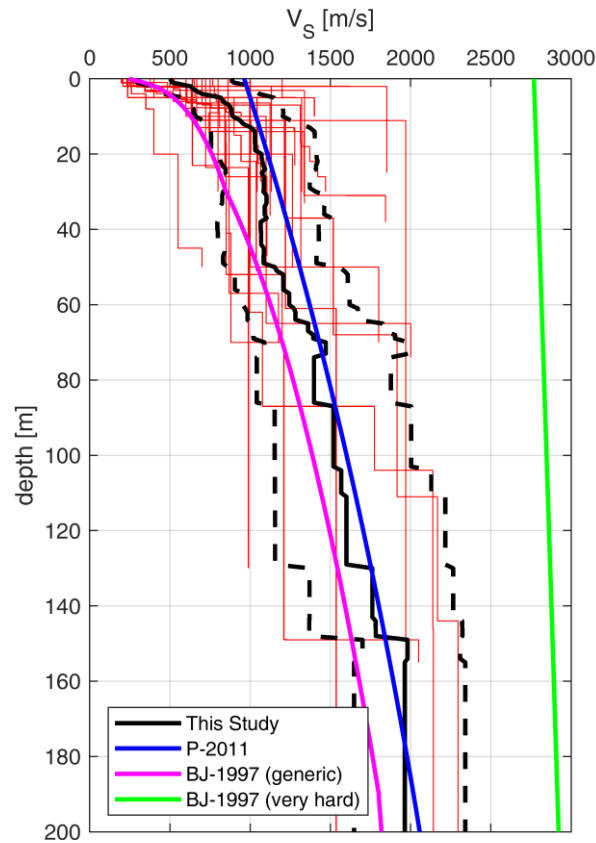
Figure 12. Mean shear-wave velocity profile (black line) and its standard deviation (dotted lines), up to 200 m, obtained from measured V_S profiles available for the selected reference rock-sites (red lines). P-2011 is the model by Poggi et al. (2011) for reference rock sites in Switzerland; BJ-1997 are the profile for generic and very hard rocks proposed by Boore and Joyner (1997) for North America.

Table 5 lists the pre-selected sites with measured $V_{S,30}$> 750 m/s but not finally selected as reference rock sites. All stations are classified as EC8-B based on detailed geological maps. The SGR (San Giorgio La Molara, southern Italy) station is characterized by a slightly peaked H/V curve (f_0~1Hz) and installation conditions that cannot be considered as free-field (inside a small building). SGIUA (San Giuliano di Puglia, southern Italy) is a temporary station with H/V broadband response and $V_{S,30}$ slightly higher than 750 m/s. LRS (Lauria, southern Italy) is installed on a steep slope and the horizontal-to-vertical spectral ratio is broadband. Finally, the AQP (L'Aquila-Pettino, central Italy) station has already been reported in the article by Lanzano et al. (2020), based on the results of the previous deliverable. In particular, "[...] the latter station shows intermediate-to-long periods amplifications with f_0 around 2 Hz and its behavior can be ascribed to topographic effect, since it is installed on a ridge with flat crest and very steep flanks (http://itaca.mi.ingv.it/ItacaNet 31/#/station/IT/AQP)".

Table 5. Pre-selected stations with measured $V_{S,30}$>750m/s, disregarded after the application of Table 3 methodology for the reference rock sites identification

Stations	VS30	HV	GEO	TOPO	HOU	Score
IT.LRS	1024	BB	EC8-B	Slope	no FF	4.5
IT.AQP	836	Peaked	EC8-B	T4*	FF	4.25
IT.SGR	849	Peaked	EC8-B	flat	no FF	3.75
IT.SGIUA	782	BB	EC8-B	flat	FF	4.25

Scaling GMMs from generic to reference rock sites

This section is focused on the calibration of a model for the prediction of elastic acceleration response spectra and Fourier amplitude spectra for reference rock sites in Italy. Given the large number of ground-motion models available in the literature (see Douglas, 2019), we prefer to compute correction factors of an existing model rather than to calibrate an *ad-hoc* model. The idea is to evaluate these factors by means of residual analysis, that models the discrepancies between ground-motion observations and reference GMM predictions. The proposed approach is similar to the Referenced Empirical Approach (REA), proposed by Atkinson (2008) for the calibration of a predictive model for Eastern North America starting from the model for active shallow crustal regions by Boore and Atkinson (2008). The REA approach is also used by Atkinson (2010) for the GMM of the volcanic earthquakes in the Hawaii Islands. The correction factor for reference rock ground-motions is $\delta(T) = log_{10}Amp$, where *Amp* is the reduction with respect to generic rock predictions. In other words, $\delta(T)$ describes the log factor that must be added (with sign) to the predictions for generic rocks to provide ground motions in agreement with the mean observations of the selected reference sites. Thus, the predicted ground-motion amplitude Y_{ref} for reference rock site is:

$$log_{10}Y_{ref}\ (T, M, R, FS) = log_{10}Y_{ITA18\text{-}800}\ (T, M, R, FS) + \delta(T) \qquad [9]$$

where the generic rock prediction ($Y_{ITA18\text{-}800}$) is dependent on period *T* (or frequency for the FAS model), moment magnitude *M*, distance *R* (R_{JB} or R_{rupt}) and style of faulting *SF*, while δ depends only on *T*. The reference models are still ITA18 for SA and FAS. The residuals $R_{e,s}$ are calculated as the logarithm differences between the observations of a subset of ITA18 dataset composed by records of reference rock sites, and the prediction of ITA18 for $V_{S,30}=800m/s$. The subset is composed of 799 records, relative to 104 sites out of the 116 selected reference rock stations.

The most important assumption in the calibration of $\delta(T)$ is that the magnitude and distance scaling of ground motions of reference rock sites is the same as that exhibited for ITA18. This underlying assumption was already verified in the works of Felicetta et al. (2018) and Lanzano et al. (2020), relative to the calibration of GMM for reference rock sites in Italy. However, in order to confirm this choice, the values of $R_{e,s}$ are plotted in Figure 13, as a function of magnitude, distance and $V_{S,30}$ for 3 representative spectral ordinates (SA-T=0.1, 0.5 and 2s).

(a)

(b)

(c)

(d)

(e)

(f)
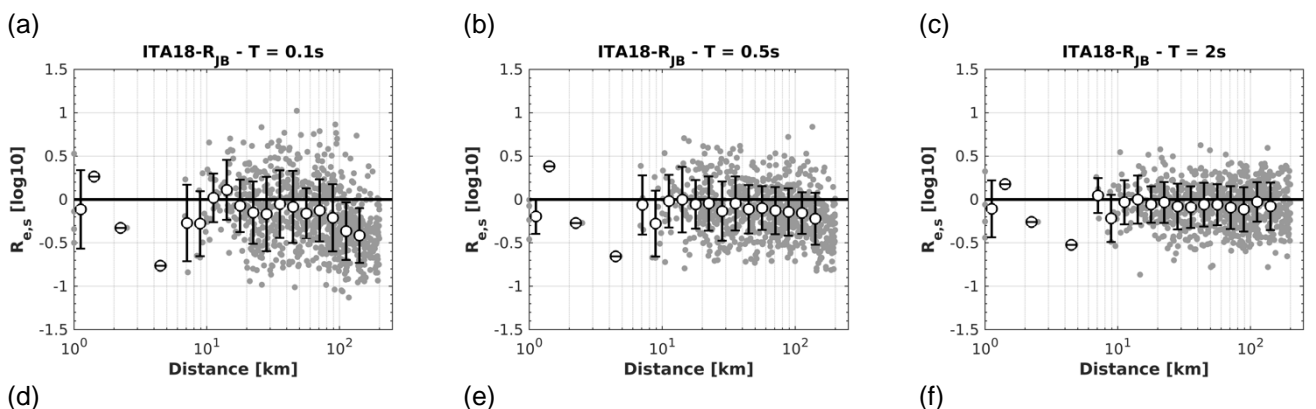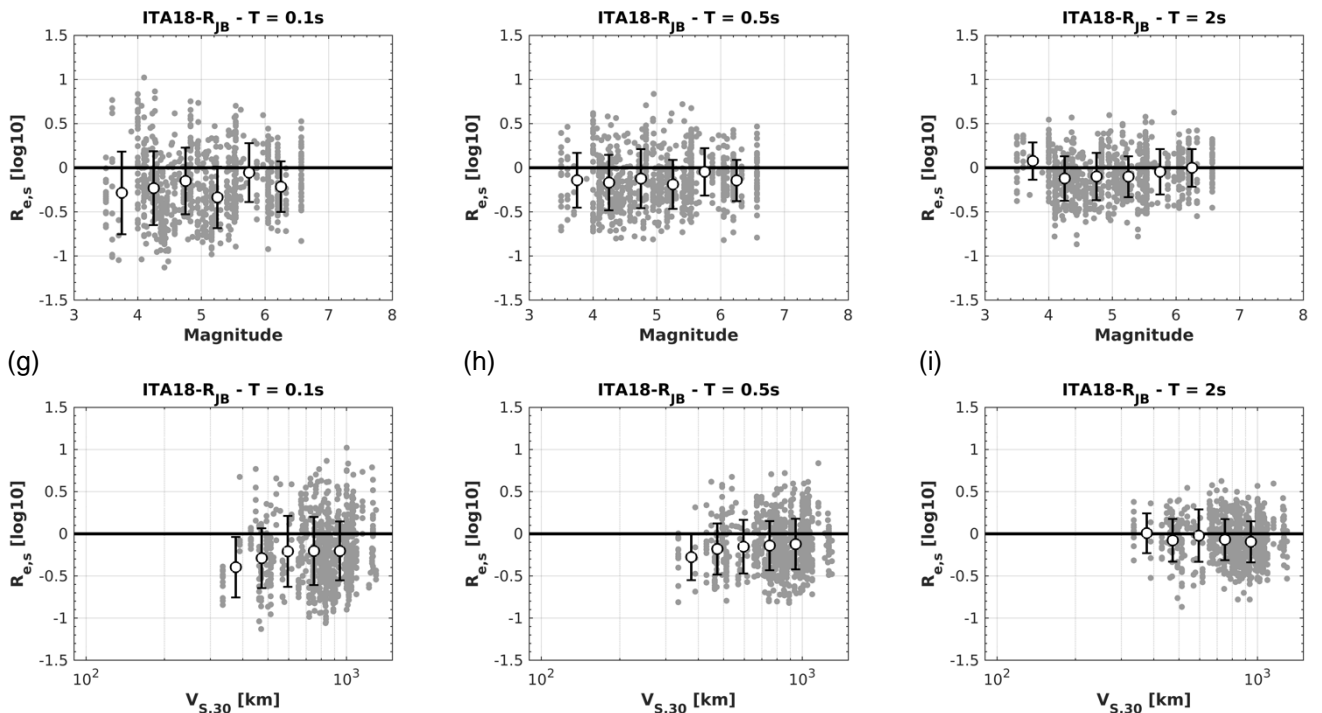
Figure 13. Logarithm differences, $R_{e,s}$, of reference rock sites observations and SA ITA18 (R_{JB}) predictions at $V_{S,30}$=800m/s: a) $R_{e,s}$ vs R_{JB} at T=0.1s; b) $R_{e,s}$ vs R_{JB} at T=0.5s; c) $R_{e,s}$ vs R_{JB} at T=2s; d) $R_{e,s}$ vs M_W at T=0.1s; e) $R_{e,s}$ vs M_W at T=0.5s; f) $R_{e,s}$ vs M_W at T=2s; g) $R_{e,s}$ vs $V_{S,30}$ at T=0.1s; h) $R_{e,s}$ vs $V_{S,30}$ at T=0.5s; i) $R_{e,s}$ vs $V_{S,30}$ at T=2s.

The residual bins are found to be negative, with an almost constant bias with magnitude, distance and $V_{S,30}$. We observe only a not negligible dependence on distance at high frequencies for the recordings at a distance exceeding 100km. Moreover, the averaged deviation from zero is reduced as period increases. As a result, δ is calculated period by period as the mean of the $R_{e,s}$. The values of the corrective terms and the associated standard deviation (σ_δ) are reported in the Appendix IV for the elastic acceleration response spectra and the Fourier spectra, both for R_{JB} and R_{rupt}. The results are also shown in Figure 14, including the standard deviations of ITA18 for comparison.
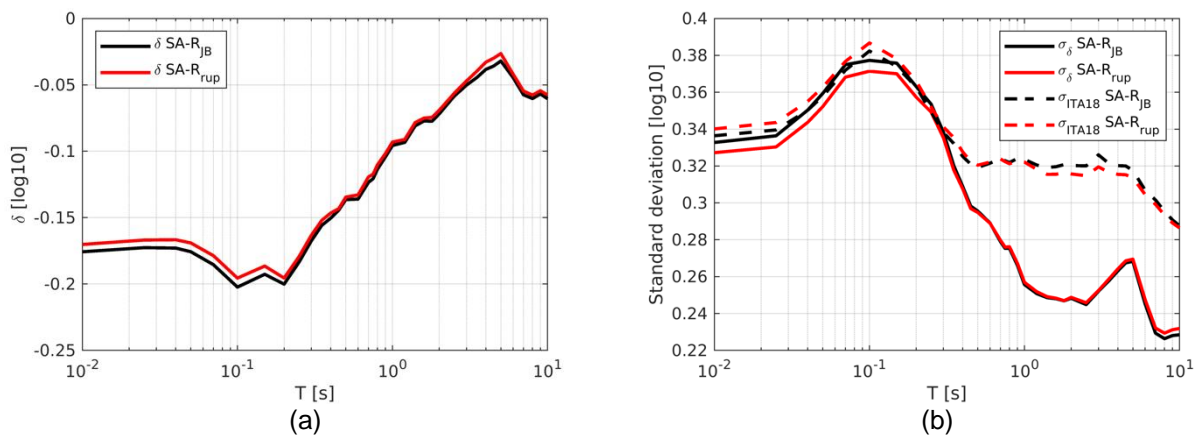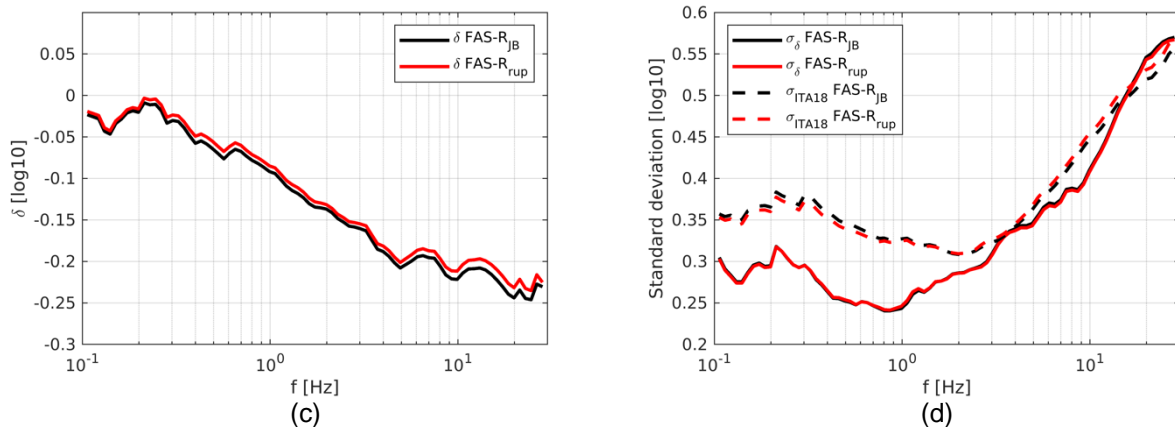
Figure 14. Period/frequency dependent corrective terms, δ, and associated standard deviations, σ_δ: a) δ for ITA18 model of SA; b) σ_δ for ITA18 model of SA; c) δ for ITA18 model of FAS; d) σ_δ for ITA18 model of FAS.

The trends of the corrective terms are very similar for FAS and SA and show a noticeable reduction of seismic motion at high frequencies with maximum values around -0.21 for SA (T=0.1-0.2s) at -0.25 for FAS (f=20-25Hz). At low frequencies, the corrections tend to become zero, with the lowest absolute values for SA at T=5s (δ=-0.04) and FAS at f=0.2Hz (δ=-0.01). Figure 15 compares the SA corrective terms of this study to the host-to-target adjustments (Campbell, 2003), which are equivalent to the scaling factor from hard (reference) to soft (generic) rock sites (HTS). The curve of Van Houtte et al. (2011) is obtained by the well-known $V_{S,30}$- κ_0 relationship proposed by the authors. The GMM for very hard rock sites calibrated by Laurendau et al. (2018) is based on the generation of a virtual rock motion dataset, obtained by the deconvolution of the surface records of the of the Kik-Net (Japanese) network. The results of our study are computed as the exponential of the reciprocal (HTS=$10^{1/\delta}$) of δ in SA shown in Figure 14a.
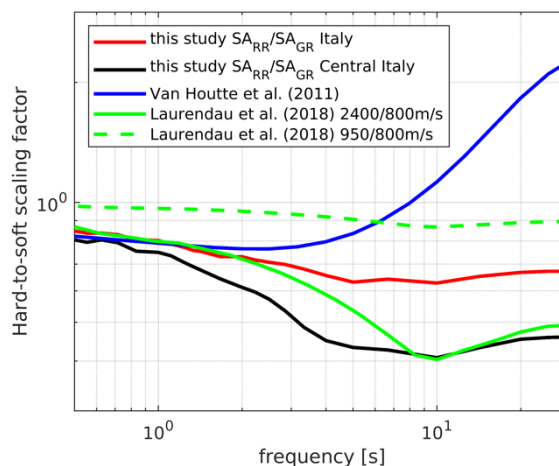
Figure 15. Hard-to-soft rocks ground motion scaling factors as a function of frequency.

At low frequencies all models show the same trend, i.e. slightly higher motion of generic rocks w.r.t. reference rocks. At high frequencies, the results are consistent with Laurendau et al. (2018), with a large frequency reduction on hard rock. If the subset of sites in central Italy is considered, the values are very similar to those obtained from the ratio between the predictions for $V_{S,30}$=2400m/s (reference) and $V_{S,30}$=800m/s (generic) of Laurendau et al. (2018). The largest hard-to-soft rocks amplifications (inverse of Amp=10^δ) in Central Italy is about 2-3 times at f=10Hz, while if we consider all the reference

rock sites is, on average, around 1.7 times. In contrast, as already stated by Laurendau et al. (2018), "[…] the classical Campbell (2003) approach coupled with the $V_{S,30}$- κ_0 relationship compiled by Van Houtte et al. (2011), predicts a high frequency increase on hard-rock (by a factor about 1.25 at 10 Hz and 2 at 30 Hz), resulting from the assumed much lower κ_0 values on very-hard rock".

In comparison to ITA18, the standard deviations of the corrections show an average reduction of about 25% at low frequencies, while they are nearly equal at high frequency. Such large standard deviation shows that seismic motion on rock and stiff-soil sites does not depend only on $V_{S,30}$, but also on other parameters, such as the high-frequency attenuation site properties. Laurendeau et al. (2013) show that once introduced this parameter in a ground motion model, the associated variability is significantly reduced.

The standard deviation associated to the spectra of reference rock sites, predicted by Eq.[9], should be obtained on the basis of the error propagation by recombining σ_{ITA18} and σ_δ and calculating the correlation coefficients between the residuals of each model; however, considering the discrepancy between the number of data used to calibrate ITA18 and the δ model and the small differences between σ_{ITA18} and σ_δ, we recommend that the standard deviation of ITA18 should still be used for reference rock sites (Figure 14b and 14d).

Figure 16 shows the comparison between the predicted spectra for the generic and reference rocks for two scenarios relevant for seismic hazard assessment (M_w 5.0 and 6.0, R_{JB}=0km, normal fault).

(a)

(b)

(c)

(d)

Lanzano G., Felicetta C., Pacor F. - Metodology to identify reference rock sites - SIGMA2-2020-D3-047
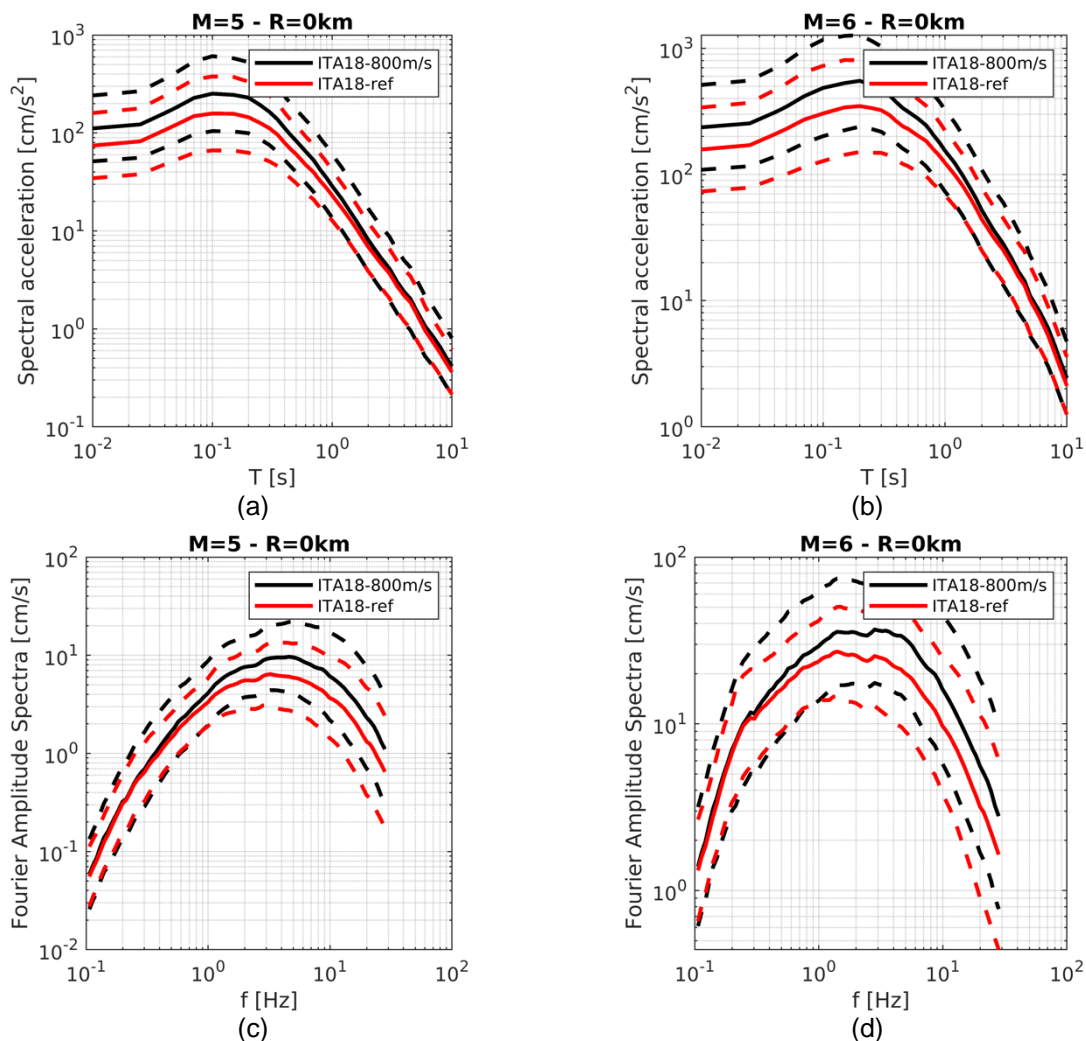
Figure 16. Predicted ITA18 spectra for $V_{S,30}$=800m/s and for reference rock sites: a) acceleration response spectra M_w=5.0 R_{JB}=0km; b) acceleration response spectra M_w=6.0 R_{JB}=0km; c) Fourier amplitude spectra M_w=5.0 R_{JB}=0km; d) Fourier amplitude spectra M_w=6.0 R_{JB}=0km;

Since the δ values are not constant with the period, the spectra for reference rock site not only decrease in amplitude but also change shape. As far as the maximum values are concerned, the T=0.2s ordinate of the SA spectrum at Mw=6.0 moves from 0.56g to 0.35g; while the Fourier spectrum, for the same scenario at f=3Hz, predicts 36cm/s and 25cm/s for generic and reference rock sites, respectively.

Based on the calibrated correction values, we compute the value of the $V_{S,30}$ which corresponds to the seismic motion level of the selected reference stations. Assuming that the scaling with $V_{S,30}$ of Eq. [4] is constant, i.e. that the value of the k coefficient does not vary (Figure 17a for SA), the "virtual" $V_{S,30}$ for the reference sites is calculated as:

$$V_{S,30-ref}(T) = 800 * 10^{\left(\frac{\delta(T)}{k(T)}\right)}$$ [10]

Figure 17b reports the $V_{S,30-ref}$ as a function of period, showing that also such parameter is period dependent: $V_{S,30-ref}$ increases from about 2500m/s at PGA (0.01s) up to 5000m/s at T=0.1s; then decreases to about 900m/s in the range T=2-5s. The high frequency $V_{S,30-ref}$ is not representative of the rocks in Italy, and such calculation still reveals the limit of this parameter in the description of ground motion of the stiff soils and rocks sites.
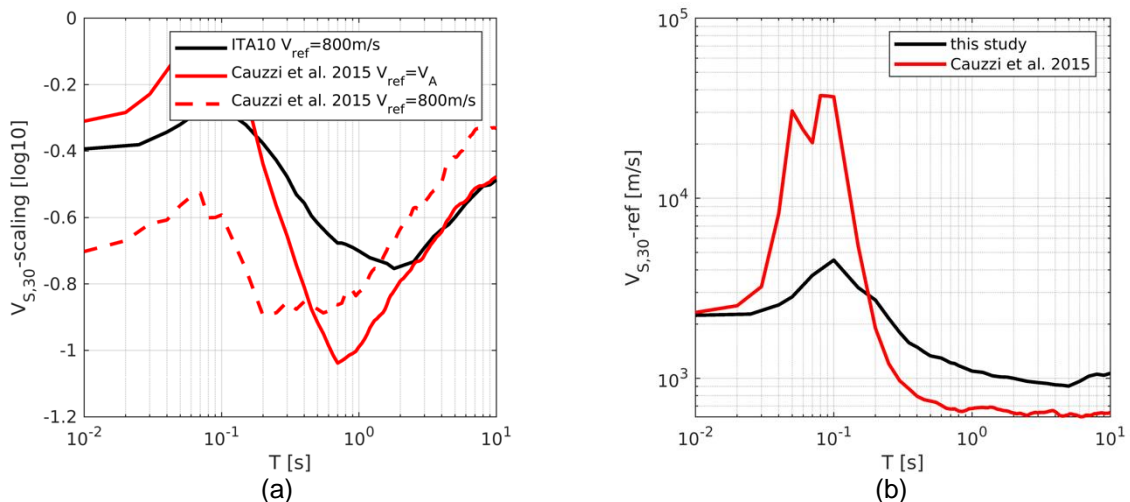
Figure 17. a) $V_{S,30}$ scaling coefficient k of ITA18-SA and Cauzzi et al. (2015) as a function of period T; b) $V_{S,30-ref}$ computed according Eq. [10] and V_A proposed by Cauzzi et al. (2015) as a function of period.

$V_{S,30-ref}$ values are also compared to the V_A proposed by Cauzzi et al. (2015), i.e. the reference shear wave velocity for bedrock; the Authors used V_A to scale the $V_{S,30}$ in the site term of the prediction model they proposed. For the sake of completeness, Figure 16a also reports the calibration coefficients of the linear $V_{S,30}$ scaling (same functional form of ITA18) by Cauzzi et al. (2015), named b_V and b_{800} for $V_{ref}=V_A$ and V_{ref}=800m/s, respectively. According to Cauzzi and Faccioli (2008), the absolute value of b_V should approach 0.5 at long periods, as $(V_A/V_{S,30})^{0.5}$ is the theoretical site amplification for very smooth V_S variation in sediments. On the other hand, $|b_V|$ should reach 1 in the period range where resonant response of sediments is expected (neglecting the density contrast).

The trend of $V_{S,30}$ scaling of ITA18 is similar to that found by Cauzzi et al. (2015), but the range of variability is smaller: from -0.2 at 0.1s to -0.75 at 2s for ITA18 and from –0.1 at 0.1s to -1 at 0.7s for Cauzzi et al. (2015). As a result, the $V_{S,30-ref}$ values (V_A) obtained by Cauzzi et al. (2015) at short periods are significantly higher than those found in our analysis, approaching un-physical values of $3*10^4$ m/s; on the contrary, at long periods, V_A is reduced down to 600 m/s.

At the end of this section we explore the possibility of building a model to parameterize the corrective term δ. We take benefit of the high frequency attenuation parameter κ_0 (Anderson and Hough, 1984) computed for reference rock sites in central Italy and reported in the first-year deliverable (SIGMA2-2019-D3-027/1). The classical approach of Anderson and Hough (1984) was used to evaluate such parameters, estimating the frequency decay of the semi-logarithm acceleration Fourier spectra. The site-specific component κ_0, representing the attenuation due to propagation in the shallower layers, was obtained using a linear model with distance for each station. Further details on this analysis are reported in the deliverable. We can employ a subset of 238 (out of 799) records of 20 reference rock stations out of the 36 sites for which κ_0 has been estimated. As a first step, we explore the $R_{e,s}$ dependence on κ_0 in Figure 18. The range of variation of κ_0 is between 0.005 and 0.05s.

(a)   (b)
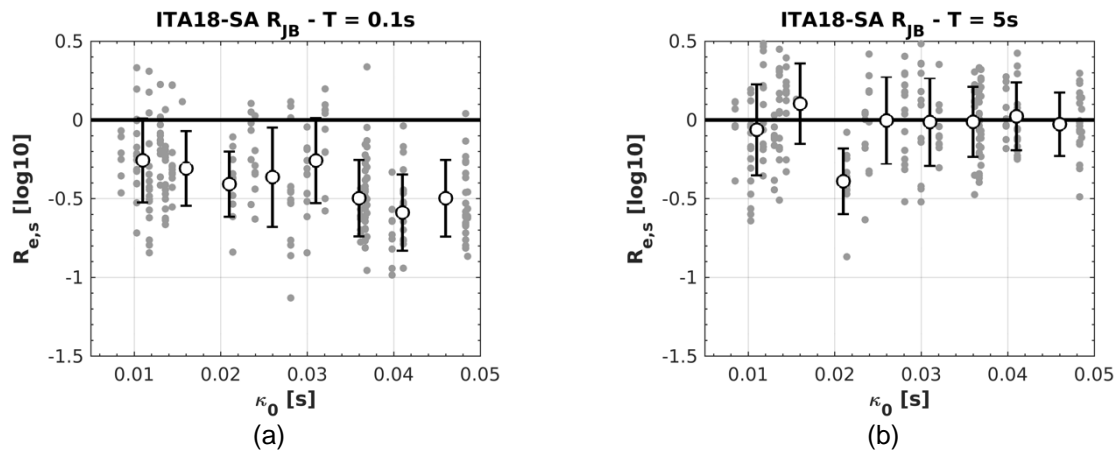
Figure 18. Residuals (logarithm differences between the observations of the reference rock sites, and the SA-R_{JB} prediction of ITA18 for $V_{S,30}$=800m/s) vs. high frequency attenuation parameter κ_0: a) T=0.1s; b) T=5s.

The logarithmic deviations of reference rock sites observations with respect to generic rock prediction shows a clear dependence on κ_0, especially at high frequency, which directs our attempt at parameterization. In particular, $R_{e,s}$ decrease as κ_0 increase, enlarging the gap between generic and reference rocks.

Following Laurendau et al. (2013), we adopt the following functional form of (T):

$$\delta(T) = a_\kappa + b_\kappa log_{10}\frac{V_{S,30}}{800} + c_\kappa \kappa_0 \quad for T \leq 0.33s \qquad [11]$$

$$\delta(T) = a_\kappa + b_\kappa log_{10}\frac{V_{S,30}}{800} \qquad for T > 0.33s \qquad [12]$$

Where a_k, b_k and c_k are period-dependent coefficients obtained from the calibration. The period limit is evaluated after the first trial calibration and is the period above which the c_k coefficient becomes positive. The corresponding threshold frequency is 3Hz and is included in the interval of f_E, the frequency range between 1 and 10 Hz, after which is usually adopted to measure κ_0 (Douglas et al., 2010). The adopted limit period is also consistent with that proposed by Laurendau et al. (2013), equal to 0.2s.

The values of such coefficients are reported in the Appendix IV. The predictions (δ_{model}) of the R_{JB} model in Eq. [9-10] are reported in Figure 19a and 19c for SA and FAS, respectively. The mean of the residuals computed over the 799 (all the reference rock stations) and 238 (the stations with κ_0 estimate) records are also reported and are named δ_{mean} (red curve) and $\delta_{mean,red}$ (black curve), respectively.
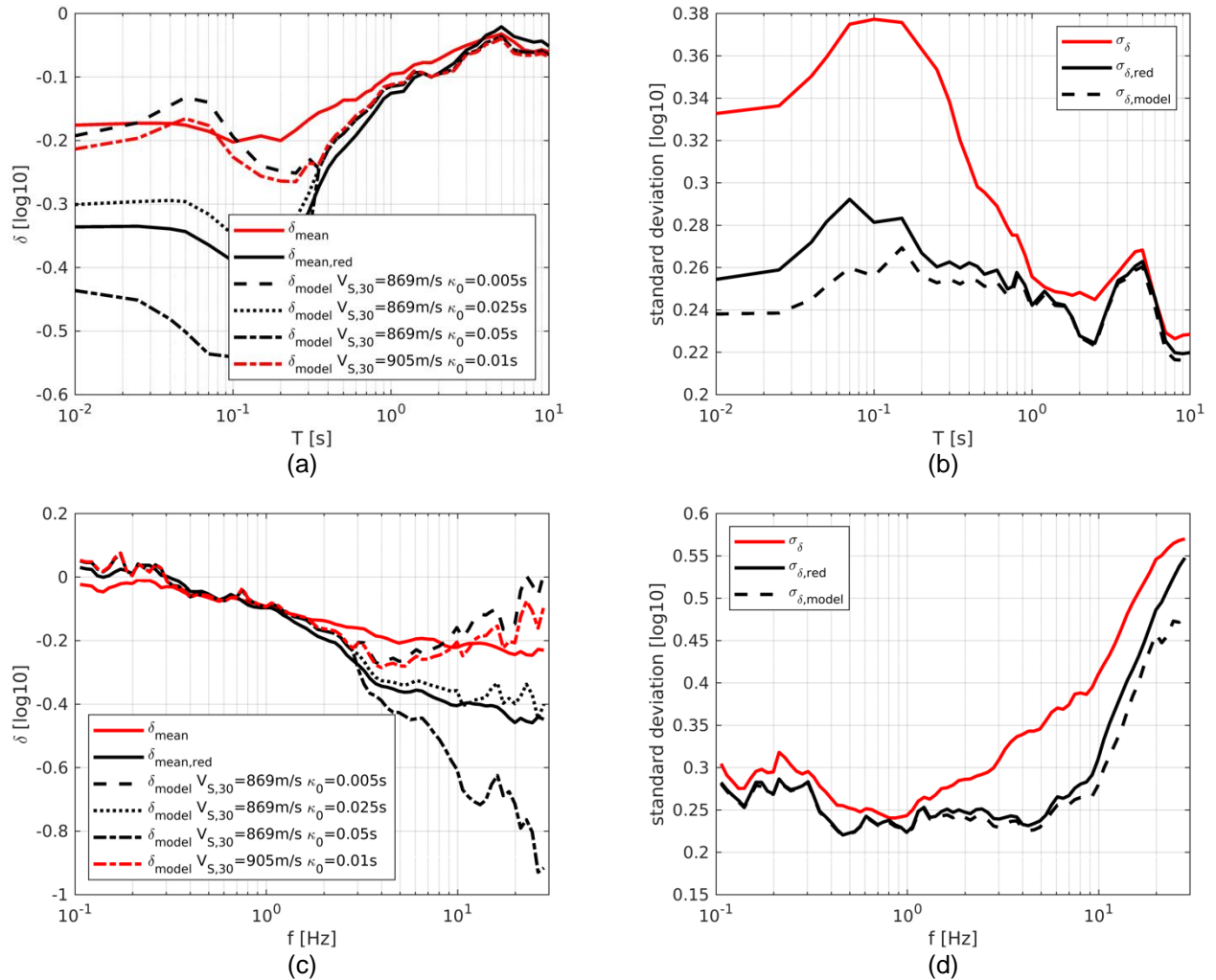
Figure 19. Outcomes of the calibration of δ in Eq. [8]: a) predictions of δ model for SA-R_{JB} as a function of period; b) standard deviations of δ model for SA-R_{JB} as a function of period; c) predictions of δ model for FAS-R_{JB} as a function of frequency; b) standard deviations of δ model for FAS-R_{JB} as a function of frequency.

The first aspect we highlight is the remarkable difference between the mean (and standard deviation) of the residuals between the "large" (799 recordings) and the "small" (238 recordings) subsets, both for SA and FAS: at high frequencies, the corrective term is wider for the small dataset, while there are no considerable differences at low frequencies. As far as variability is concerned (Figure 19b and 19d), a reduction up to 25% of sigma at high frequencies is observed for both SA and FAS. This difference is related to the "local" character of the "small" dataset consisting only of sites in central Italy. Extending the analysis to the whole of Italy, we also include sites characterized by more rigid rocks with higher $V_{S,30}$ values.

Although the "small" subset could be rather limited, the calibration allows identification of a significant dependence on κ_0 in the available data range; in particular, the predictions for $V_{S,30}$=869m/s,

corresponding to the mean of measured $V_{S,30}$ of the reference sites in Central Italy (SIGMA2-2019-D3-027/1), and three different values of κ_0 (0.005, 0.025 and 0.05s) are reported. At high frequencies (up to 0.3s for SA and from 3Hz onwards for FAS), the c_κ coefficient (scaling with κ_0) is negative and this determines a remarkable reduction of seismic motion for the sites with the highest κ_0; at low frequencies c_κ values are zero, resulting in no change of δ. It is noted, in particular, that κ_0 =0.025s reproduces the mean curve and can be considered as a representative value for the reference rock sites in central Italy: this value is reconfirmed by the averaged value of κ_0 calculated for such reference sites equal to 0.022s. We also include the prediction for $V_{S,30}$=905m/s, corresponding to the mean of measured $V_{S,30}$ of all the reference sites in Italy (§ 4.0), and, in this case, we observe a rough fit with the mean of the "large" subset adopting κ_0 =0.01s. The latter can be considered as a preliminary averaged target value for the reference rock site in Italy.

Discussion and conclusions

The main objective of this work was to apply the methodology developed last year to identify seismic reference rock stations in Central Italy, to the whole Italian territory. The Reference-Rock Identification Method (RRIM) is based on two elements: 1) the identification of site parameters representing the reference site conditions and 2) the construction of the scoring scheme to classify candidate stations.

The set of proxies is composed by six parameters: three are related to the analysis of geophysical and seismological data (site term from residual analysis, resonance frequencies from Horizontal-to-Vertical spectral ratios, time-average shear-wave velocity in the first 30m); the remaining ones concern geomorphological and installation features (outcropping rocks or stiff soils, flat topography and absence of interaction with structures). Following the Decision Matrix Method (DDM), that is a qualitative technique used to rank the multi-dimensional alternatives of an option set, RRIM introduces a decision matrix consisting in a set of criteria, weighted in order of relevance, scored and summed to gain a total score. DDM is suitable for the identification of reference sites, since some of the proxies are not measurable (such as the geological map) and cannot be easily combined with the others. In order to handle the relevance, the data quality and the possible lacking of information, to each proxy the RRIM weighting scheme is given by the combination of two indicators assigned to each proxy: the hierarchical index (HI), variable from 0.5 to 2, and the proxy weight (PW), ranging from 0 to 1. The former quantifies the relevance of the site parameter to represent the site response (i.e $V_{S,30}$, surface geology and resonance frequency), the latter takes into account the presence (or absence) and the quality of the information. In this work, we apply the RRIM to a very large dataset, extracted from the last release of Italian Accelerometric Archive (ITACA v3.1), composed by more than 1600 stations (Table 6, ITACA dataset). Given the large number of sites, the pre-selection of candidates is performed via residual analysis, selecting those with flat site response and amplitude similar or lower than the one for the generic rocks ($V_{S,30}$=800m/s). At the aim, we calibrated a GMM in Fourier amplitudes, using the same functional forms and dataset (Table 6, ITA18 dataset) adopted for the reference Italian model, valid for response spectra.

Table 6. Datasets used in this work

Dataset	# records	# stations	# events
ITA18	5607	1657	146
ITACA	32600	1716	1756
δ calibration	799	104	105

The 433 candidate stations were ranked using the scoring scheme of Table 3, with a threshold value of 4.75, with respect a maximum of 8. A total of 116 reference rock stations were identified, mainly installed along the Apennine chain, and in the areas of Hyblaean Mountains (Sicily), Gargano Promontory (Puglia) and Garda Lake (Lombardy). The associated mean $V_{S,30}$ is equal to 905m/s, if only measured values are considered. The list includes the majority of stations already identified in Central Italy (SIGMA2-2019-D3-027/1), based on a different dataset and reference GMPEs, confirming the robustness of the proposed approach.

A possible limit of the procedure could be the choice of the reference GMM for the computation of the residuals that could seem arbitrary. Compared to the previous deliverable (SIGMA2-2019-D3-027/1), a different reference model (ITA18 vs ITA10) has been used and the selected stations are nearly the same. However, to further reinforce this conclusion, we computed the residuals using two of the models developed within RESORCE (Akkar et al. 2014a), i.e. Bindi et al.(2014) and Akkar et al. (2014b) models, using the ITACA dataset. Since GMMs contribute to the definition of reference sites only in the δS2S proxy, we tested the impact of using different prediction models only in the pre-selection phase. Figure 20 shows the cluster analysis (using the same number of clusters) for the two RESORCE models for SA, highlighting the pre-selected clusters: in both cases a cluster with a flat and de-amplified trend over frequency is evident; while the set B of Bindi et al. (2014) show a small amplification at high frequencies. In the latter case, an additional cluster of "outliers" emerges, characterized by amplifications at low frequencies much greater than 7. The clusters obtained from the residuals computed using the model by Akkar et al. (2014b) are, instead, very similar to those obtained using ITA18 (Figure 8b).
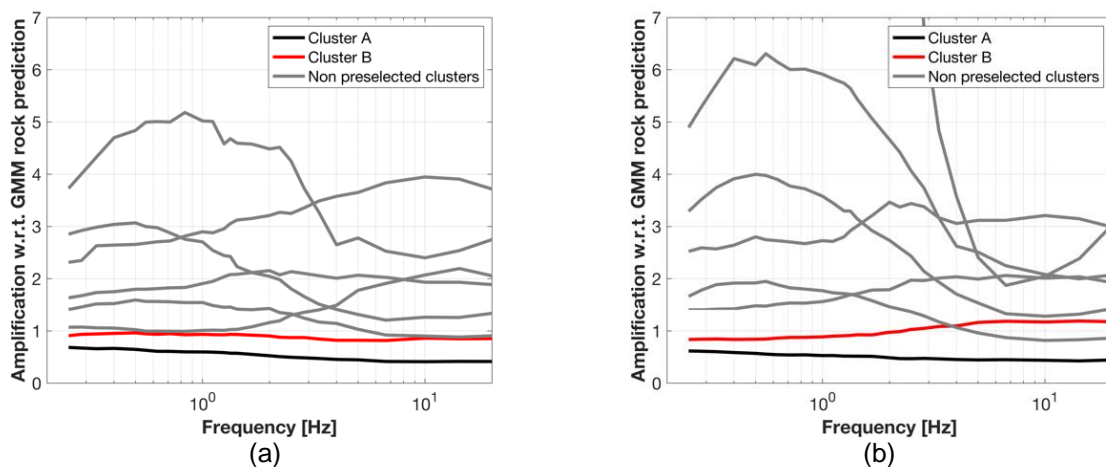
Figure 20. Cluster analysis of $e^{\delta S2S}$, computed using the RESORCE GMMs for SA in hypocentral distance: a) Akkar et al. (2014b); Bindi et al. (2014). Cluster A and B are considered for station pre-selection.

The total number of pre-selected stations (cluster A and B) is 440 and 546 for Akkar et al. (2014) and Bindi et al. (2014), respectively: the stations in common with those pre-selected using ITA18 are 410 (83%) and 454 (92%), respectively. After the application of the methodology in Table 3, the number of the selected reference rock sites slightly reduce w.r.t. ITA18 selection, losing 2 and 9 sites for Bindi et al 2014 and Akkar et al. 2014 selections, respectively. It can be concluded that using several GMMs an average 5% change in the number of selected reference sites can occur.

ITACA dataset includes about 800 records of the 116 selected reference rock sites that are used to calibrate the empirical corrective terms (Table 6), suitable to scale the generic rock ground motion level to the reference one. The trends of such generic-to-reference rock factors are similar to those proposed by several authors in literature for host-to-target adjustment factors. The impact of the introduction of

empirical corrective factors is evaluated in Table 7, by means of the normalized difference between the median predictions of the ITA18 at $V_{S,30}$=800m/s and ITA18-ref (according to Eq.[7]). Similar percentage reductions are reported for the model of Felicetta et al. (FEL18, 2018), computed with respect to Bindi et al. (ITA10, 2010) and for the Central Italy model (CI19, 2019), as discussed in the previous deliverable and updated in the paper by Lanzano et al. (2020).

Table 7. Percentage reduction between the predictions of generic and reference rock sites. The results are updated after Lanzano et al. (2020).

ΔY (%)	PGA	SA-T=0.1s	SA-T=0.2s	SA-T=1s	SA-T=2s
This study-SA R_{JB}	33.9	38.1	38.0	20.2	16.1
Lanzano et al. (2020)	40.5	46.7	36.7	4.2	6.9
Felicetta et al. (2018)	35.1	33.5	38.5	26.5	28.0

The trend of the reduction is quite consistent with the previous studies. This is largest at SA-T=0.1s and diminishes at long periods down to 16%. Figure 21 shows the spectra predicted at different scenarios for the reference conditions of ITA18-ref, FEL18 e CI19, including the associated variability. We use the total variability of ITA18 for reference rock site predictions.

(a)

(b)

(c)

(d)

Lanzano G., Felicetta C., Pacor F. - Metodology to identify reference rock sites - SIGMA2-2020-D3-047
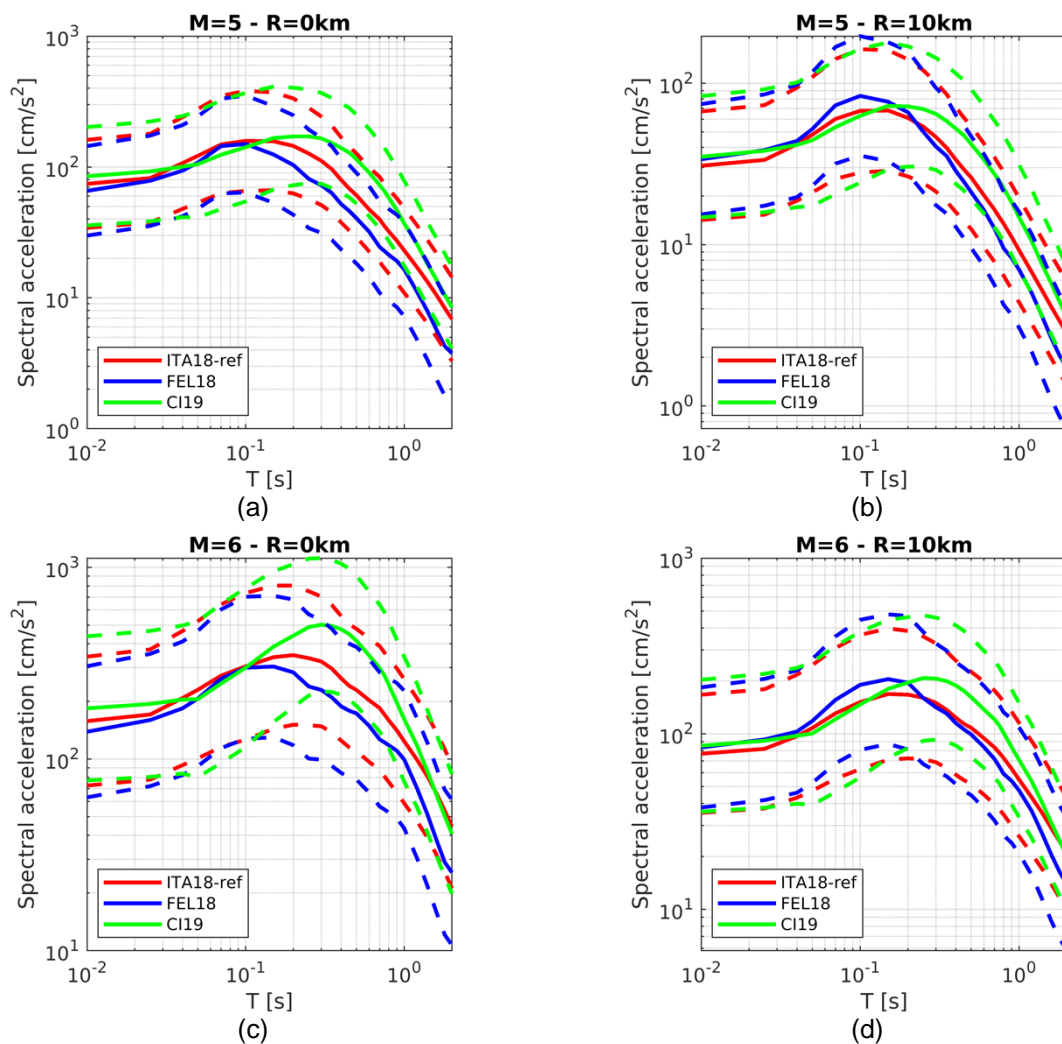
Figure 21. Acceleration response spectra (5% damping) predicted by ITA18-ref (this study), CI19 (Lanzano et al. 2020) and FEL18 (Felicetta et al. 2018) for several scenarios: a) M_W=5.0 R_{JB}=0km; b) M_W=5.0 R_{JB}=10km; c) M_W=6.0 R_{JB}=0km; d) M_W=6.0 R_{JB}=10km. The style of faulting is normal.

The predictions of the three models are quite similar at low frequencies; at long periods the ordinates of the model proposed in this analysis is higher than FEL18, but lower than those proposed by CI19. As a matter of fact, the spectra of CI19 reflect the rich low frequency energy content (T>0.5s) of the records of the events in this small area (Lanzano et al. 2016; Bindi et al. 2019).

We also try to compute the value of the $V_{S,30}$ which corresponds to the seismic motion level of the selected reference stations ($V_{S,30-ref}$). As well as returning large values of $V_{S,30-ref}$ this calculation also leads to period-dependent values, which is not possible as $V_{S,30}$ is a period-independent parameter. An alternative approach and the possible prosecution of this research could be the application of the quarter-wavelength method (Joyner and Fumal, 1984; Poggi et al., 2011), by calculating the quarter-wavelength velocity, which is a period dependent parameter.

Finally, we attempted to model the empirical corrective factors, with a parametric form depending on $V_{S,30}$ and κ_0 (Eqs. [9-10]), using the attenuation values estimated for reference rock sites in central Italy. We used such a model to correct the ITA18 predictions for the reference rock acceleration response spectra at different scenarios in Figure 22.

(a)   (b)
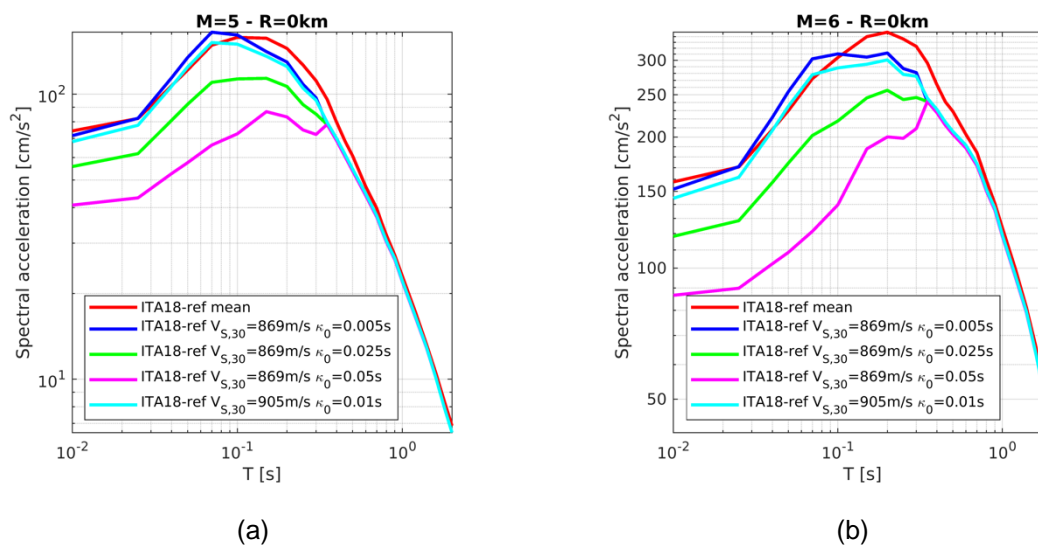
Figure 22. Acceleration response spectra (5% damping) predicted by ITA18-ref, incorporating the model of Eqs.[9-10]: a) M_W=5.0 R_{JB}=0km; c) M_W=6.0 R_{JB}=0km. The style of faulting is normal.

The introduction of the high frequency attenuation parameter dependency allows to additionally reduce the spectral amplitudes as κ_0 increases and to shift the SA peak value to shorter periods.

RRIM was able to identify 116 reference rock sites in Italy, not affected by amplifications, over a wide range of frequencies. However, such stations have remarkably different behaviours at high-frequencies, ranging the estimates of κ_0 from 0.0074s for LSS to 0.045 for SACR. As a consequence, the parameter κ_0 should be explicitly considered in the selection of reference sites to avoid too lower values with large dispersion in the high frequency prediction.

The wide variability of κ_0, observed among the reference sites seems to have a regional dependence and deserves to be investigated. Indeed, the average reference rock amplitude of seismic motion in central Italy is different from the one estimated in the entire country (Figure 18 and Figure 21) probably

due to the stronger attenuation properties of the superficial layers in central Italy. One of the future developments could focus on the study of the regional characteristics of the high frequency attenuation parameter with the aim of reproducing a map similar to the one proposed by Van Houtte et al. (2018) for New Zealand.

In conclusion, the definition of the "ideal" reference site on the basis of the proxies proposed by the RRIM, could be not sufficient, since the high frequency attenuation parameter must also be controlled. The calibration of corrective factors depending on the pair $V_{S,30}$ - κ_0, will allow to assess the ground motion with respect to a reference site defined a priori (i.e. the "ideal" one), corresponding to specific values of κ_0 and $V_{S,30}$, conventionally selected (for example vs30 = 1000m/s and κ_0 =0.01s).

Reference

Abrahamson, N. A., Schneider, J. F., & Stepp, J. C. (1991). Empirical Spatial Coherency Functions for Application to Soil-Structure Interaction Analyses. Earthquake Spectra, 7(1), 1–27. https://doi.org/10.1193/1.1585610

Akkar, S., Sandıkkaya, M.A., Şenyurt, M., Sisi, A.A., Ay, B.Ö., Traversa, P., Douglas, J., Cotton, F., Luzi, L., Hernandez, B. and Godey, S., 2014a. Reference database for seismic ground-motion in Europe (RESORCE). Bulletin of earthquake engineering, 12(1), pp.311-339.

Akkar, S., Sandıkkaya, M.A. and Bommer, J.J., 2014b. Empirical ground-motion models for point-and extended-source crustal earthquake scenarios in Europe and the Middle East. Bulletin of earthquake engineering, 12(1), pp.359-387.

Anderson John G., Hough Susan E. (1984) A model for the shape of the fourier amplitude spectrum of acceleration at high frequencies. Bulletin of the Seismological Society of America 74 (5): 1969–1993. doi: https://doi.org/

Al-Atik, L., N. A. Abrahamson, J. J. Bommer, F. Scherbaum, F. Cotton, and N. Kuehn (2010). The variability of ground-motion prediction models and its components, Seismol. Res. Lett. 81(5) 794–801.

Atkinson, G.M. (2008). Ground-motion prediction equations for eastern North America from a referenced empirical approach: Implications for epistemic uncertainty. Bulletin of the Seismological Society of America, 98(3), pp.1304-1318.

Atkinson, G. M. (2010). Ground-motion prediction equations for Hawaii from a referenced empirical approach. Bulletin of the Seismological Society of America, 100(2), 751-761.

Bates, D., M. Mächler, B. Bolker, and S. Walker (2015). Fitting linear mixed-effects models using lme4, J. Stat. Software 67(1) 1-48.

Bindi, D., Picozzi, M., Spallarossa, D., Cotton, F., & Kotha, S. R. (2019a). Impact of Magnitude Selection on Aleatory Variability Associated with Ground- Motion Prediction Equations: Part II—Analysis of the Between- Event Distribution in Central Italy. *Bulletin of the Seismological Society of America*, *109*(1), 251-262.

Bindi, D., Kotha, S.R., Weatherill, G., Lanzano, G., Luzi, L. and Cotton, F., (2019b). The pan-European engineering strong motion (ESM) flatfile: consistency check via residual analysis. Bulletin of Earthquake Engineering, 17(2), pp.583-602.

Bindi, D., Massa, M., Luzi, L., Ameri, G., Pacor, F., Puglia, R. and Augliera, P., 2014. Pan-European ground-motion prediction equations for the average horizontal component of PGA, PGV, and 5%- damped PSA at spectral periods up to 3.0 s using the RESORCE dataset. Bulletin of Earthquake Engineering, 12(1), pp.391-430.

Bindi D, Pacor F, Luzi L, Puglia R, Massa M, Ameri G, Paolucci R (2011). Ground motion prediction equations derived from the Italian strong motion database. Bulletin of Earthquake Engineering, 9(6), 1899-1920. http://dx.doi.org/10.1007/s10518-011-9313-z

Bommer, J.J., J. Douglas and F.O. Strasser (2003). Style-of-faulting in Ground-Motion Prediction Equations, Bull. Earthq. Eng. 1, 171-203.

Bonnefoy-Claudet S, Köhler A, Cornou C, Wathelet M, Bard PY (2008) Effects of love waves on microtremor H/V ratio. Bull Seismol Soc Am 98(1):288–300

Boore D. M. Joyner W. B. (1997). Site amplifications for generic rock sites, Bulletin of the Seismological Society of America 87, 327-341.

Boore, D., and G. Atkinson (2008). Ground-motion prediction equations for the average horizontal component of PGA, PGV, and 5%-damped SA at spectral periods between 0.01 s and 10.0 s, Earthquake Spectra 24, 99–138.

Bora, S. S., Scherbaum, F., Kuehn, N., Stafford, P., & Edwards, B. (2015). Development of a response spectral ground- motion prediction equation (GMPE) for seismic- hazard analysis from empirical Fourier spectral and duration models. Bulletin of the Seismological Society of America, 105(4), 2192-2218.

BSSC (2003). NEHRP Recommended Provisions for Seismic Regulations for New Buildings and Other Structures (Fema 450).

Campbell, K. W. (2003). Prediction of strong ground motion using the hybrid empirical method and its use in the development of ground- motion (attenuation) relations in eastern North America, Bull. Seismol. Soc. Am. 93, 1012–1033.

Cauzzi, C., & Faccioli, E. (2008). Broadband (0.05 to 20s) prediction of displacement response spectra based on worldwide digital records. Journal of Seismology, 12(4), 453.

Cauzzi, C., Faccioli, E., Vanini, M., & Bianchini, A. (2015). Updated predictive equations for broadband (0.01–10 s) horizontal response spectra and peak ground motions, based on a global dataset of digital acceleration records. Bulletin of Earthquake Engineering, 13(6), 1587-1612.

CS.LL.PP - DM 17 Gennaio 2018. Norme Tecniche per le Costruzioni. Gazzetta Ufficiale della Repubblica Italiana n. 42; 2018. (in Italian).

D' Amico M., Lanzano G., Santulin M., Puglia R., Felicetta C., Tiberti M.M., Gomez A.A., Russo E. (2018). Hybrid GMPEs for region-specific PSHA in Southern Italy. Geosciences, 8(6), 217; DOI: 10.3390/geosciences8060217.

D'Amico M., Felicetta C. Russo E., Sgobba S., Lanzano G., Pacor F., Luzi L. (2020). Italian Accelerometric Archive v 3.1 - Istituto Nazionale di Geofisica e Vulcanologia, Dipartimento della Protezione Civile Nazionale. doi: 10.13127/itaca.3.1.

David A., Vassilvitskii, S. (2007). "k-means++: the advantages of careful seeding". Proceedings of the eighteenth annual ACM-SIAM symposium on Discrete algorithms. Society for Industrial and Applied Mathematics Philadelphia, PA, USA. pp. 1027–1035.

Di Capua, G., Lanzo, G., Pessina, V., Peppoloni, S. and Scasserra, G., 2011. The recording stations of the Italian strong motion network: Geological information and site classification. Bulletin of Earthquake Engineering, 9(6), pp.1779-1796.

Ditommaso R., Mucciarelli M., Gallipoli M.R., Ponzo F.C. (2010) Effect of a single vibrating building on free-field ground motion: numerical and experimental evidences.Bull Earthquake Eng 8:693–703 DOI 10.1007/s10518-009-9134-5

Douglas, J., P. Gehl, L. Bonilla, and C. Gélis (2010). A κ model for mainland France, Pure Appl. Geophys. 167, no. 11, 1303–1315.

Douglas, J. (2019), Ground motion prediction equations 19642019, http://www.gmpe.org.uk.

Ekström, G., M. Nettles, and A. M. Dziewonski (2012). The global CMT project 2004-2010: Centroid-moment tensors for 13,017 earthquakes, Phys. Earth Planet. Inter. 1(9) 200-201.

Felicetta C., Lanzano G., D'Amico M., Puglia R., Luzi L., Pacor F. (2018). Ground motion model for reference rock sites in Italy. Soil Dynamics and Earthquake Engineering, 110, 276-283, DOI: 10.1016/j.soildyn.2018.01.024.

Felicetta, C., M. D'Amico, G. Lanzano, R. Puglia, E. Russo, and L. Luzi (2017). Site characterization of Italian accelerometric stations, Bull. Earthq. Eng. 15, no. 6, 2329–2348.

Forte, G., Chioccarelli, E., De Falco, M., Cito, P., Santo, A., & Iervolino, I. (2019). Seismic soil classification of Italy based on surface geology and shear-wave velocity measurements. Soil Dynamics and Earthquake Engineering, 122, 79-93.

Gallipoli MR, Mucciarelli M, Castro RR, Monachesi G, Contri P. Structure, soil–- structure response and effects of damage based on observations of horizontal-to-vertical spectral ratios of microtremors. Soil Dyn Earthq Eng 2004;24(6):487–95. http://dx.doi.org/10.1016/j.soildyn.2003.11.009.

Gorini A., Nicoletti M., Marsan P., Bianconi R., De Nardis R., Filippi L., Marcucci S., Palma F., Zambonelli E. (2010). The Italian strong motion network. Bull Earthquake Eng (2010) 8: 1075. https://doi.org/10.1007/s10518-009-9141-6

Grünthal, G., and R. Wahlström (2012). The European-Mediterranean Earthquake Catalogue (EMEC) for the last millennium, J. Seismol. 16(3) 535–570.

Hassani, B., Yong, A., Atkinson, G. M., Feng, T., & Meng, L., 2019. Comparison of site dominant frequency from earthquake and microseismic data in California, *Bull. Seismol. Soc. Am.*, 109(3), 1034-1040.

Joyner WB, Fumal TE (1984): Use of measured shear-wave velocity for predicting geologic and site effects on strong ground motion. 8th World Conference on Earthquake Engineering 8WCEE, San Francisco, USA, 2, 777-783.

Konno, K., and T. Ohmachi (1998). Ground-motion characteristics estimated from spectral ratio between horizontal and vertical components of microtremor, Bull. Seismol. Soc. Am. 88, 228–241.

Kotha, S. R., Cotton, F., & Bindi, D. (2018). A new approach to site classification: Mixed-effects Ground Motion Prediction Equation with spectral clustering of site amplification functions. Soil Dynamics and Earthquake Engineering, 110, 318-329.

Lanzano G., Luzi L., Pacor F., Felicetta C., Puglia R., Sgobba S., D'Amico M. (2019a). A revised ground motion prediction model for shallow crustal earthquakes in Italy. Bulletin of the Seismological Society of America, 109(2), 525-540, DOI: 10.1785/0120180210.

Lanzano G., S. Sgobba, L. Luzi, R. Puglia, F. Pacor, C. Felicetta, M. D'Amico, F. Cotton, and D. Bindi (2019b). The pan-European Engineering Strong-motion (ESM) flatfile: compilation criteria and data statistics, Bull. Earthq. Eng. 17(2), 561–582.

Lanzano G., Luzi L., Pacor F., Puglia R., Felicetta C., D'Amico M., Sgobba S., (2019c). Update of the ground motion prediction equations for Italy. Proceedings of the 7th International Conference on Earthquake Geotechnical Engineering, 17 - 20 June, Roma, Italy.

Lanzano G., Felicetta C., Pacor F., Spallarossa D., Traversa P. (2020). Methodology to identify the reference rock sites in regions of medium-to-high seismicity: an application in Central Italy. Geophysical Journal International (submitted).

Lanzano G., D'amico M., Felicetta C., Puglia R., Luzi L., Pacor F., Bindi D. (2016) Ground- Motion Prediction Equations for Region- Specific Probabilistic Seismic- Hazard Analysis , Bulletin of the Seismological Society of America , /106 (2016), https://doi.org/10.1785/0120150096

Laurendeau, A., Cotton, F., Ktenidou, O. J., Bonilla, L. F., & Hollender, F. (2013). Rock and stiff- soil site amplification: Dependency on $V_{S,30}$ and kappa (κ_0). Bulletin of the Seismological Society of America, 103(6), 3131-3148.

Laurendeau, A., Bard, P.Y., Hollender, F., Perron, V., Foundotos, L., Ktenidou, O.J. and Hernandez, B., 2018. Derivation of consistent hard rock (1000< V S< 3000 m/s) GMPEs from surface and down-hole recordings: analysis of KiK-net data. Bulletin of Earthquake Engineering, 16(6), pp.2253-2284.

Lermo J, Chávez-García FJ (1993) Site effect evaluation using spectral ratios with only one station. Bull Seismol Soc Am 83:1574–1594

Luzi L., Pacor F., Lanzano G., Felicetta C., Puglia R., D'Amico M. (2019). 2016-2017 Central Italy seismic sequence: strong-motion data, seismic hazard and design earthquakes for the seismic microzonation. Bulletin of Earthquake Engineering.

Luzi L, Puglia R, Russo E, D'Amico M, Felicetta C, Pacor F, Lanzano G, Çeken U, Clinton J, Costa G, Duni L, Farzanegan E, Gueguen P, Ionescu C, Kalogeras I, Özener H, Pesaresi D, Sleeman R, Strollo A, Zare M (2016) The Engineering strong motion database: a platform to access Pan-European accelero- metric data. Seismol Res Lett 87(4):987–997.

Luzi, L., Hailemikael, S., Bindi, D., Pacor, F., Mele, F., & Sabetta, F. (2008). ITACA (ITalian ACcelerometric Archive): a web portal for the dissemination of Italian strong-motion data. *Seismological Research Letters*, *79*(5), 716-722.

Nakamura Y (1989) A method for dynamic characteristics estimation of subsurface using microtremor on the ground surface. QR Railw Tech Res Inst 30:25–33

Pacor, F., Paolucci, R., Luzi, L., Sabetta, F., Spinelli, A., Gorini, A., ... & Dolce, M. (2011). Overview of the Italian strong motion database ITACA 1.0. *Bulletin of Earthquake Engineering*, *9*(6), 1723-1739.

Poggi, V., Edwards, B. and Fäh, D., 2011. Derivation of a reference shear-wave velocity model from empirical site amplification. *Bulletin of the Seismological Society of America*, 101(1), pp.258-274.

Pondrelli S. and Salimbeni S., Regional Moment Tensor Review: An Example from the European Mediterranean Region. In Encyclopedia of Earthquake Engineering (pp. 1-15), http://link.springer.com/referenceworkentry/10.1007/978-3-642-36197-5_301-1, Springer Berlin Heidelberg, 2015.

Priolo E., Pacor F., Spallarossa D., Milana G., Laurenzano G., Romano M.A., Felicetta C., Hailemikael S., Cara F., Di Giulio G, Ferretti G., Barnaba C., Lanzano G., Luzi L., D'Amico M., Puglia R., Scafidi D., Barani S., De Ferrari R., Cultrera G. (2019). Seismological analyses of the seismic microzonation of 138 municipalities damaged by the 2016–2017 seismic sequence in Central Italy Bulletin of Earthquake Engineering https://doi.org/10.1007/s10518-019-00652-x

Puglia R., Russo E., Luzi L., D'Amico M., Felicetta C., Pacor F., Lanzano G. (2018). Strong-motion processing service: a tool to access and analyse earthquakes strong-motion waveforms. Bull Earthquake Eng. https://doi.org/10.1007/s10518-017-0299-z.

Puglia R., Albarello D., Gorini A., Luzi L., Marcucci S., Pacor F. (2011) Extensive characterization of Italian accelerometric stations from single-station ambient-vibration measurements. Bull Earthquake Eng (2011) 9:1821–1838 DOI 10.1007/s10518-011-9305-z

Pugh S. (1981) Concept selection: a method that works. In: Hubka, V. (ed.), Review of design methodology. Proceedings international conference on engineering design, March 1981, Rome. Zürich: Heurista, 1981, blz. 497 – 506.

Régnier, J. et al. (2016). International benchmark on numerical simulations for 1D, nonlinear site response (PRENOLIN): Verification phase based on canonical cases. Bulletin of the Seismological Society of America, 106(5), pp.2112-2135.

Scognamiglio, L., E. Tinti and A. Michelini (2009). Real-time determination of seismic moment tensor for the Italian region. Bull. Seismol. Soc. Am. 99(4) 2223-2242.

Stafford, P. J. (2014). Crossed and nested mixed- effects approaches for enhanced model development and removal of the ergodic assumption in empirical ground- motion models. Bulletin of the Seismological Society of America, 104(2), 702-719.

Stehly, L., Campillo, M. & Shapiro, N.M., 2006. A study of the seismic noise from its long-range correlation properties, *J. Geoph. Res.*, 111, 1-12.

Stewart P, Fenves L, Seed B. Seismic soil-structure interaction in buildings. I: analytical methods. J Geotech Geoenviron Eng 1999;125(1):26–37. http://dx.doi.org/10.1061/(ASCE)1090-0241(1999)125:1(26).

Tibshirani R., Walther G., Hastie T. (2001). Estimating the number of clusters in a data set via the gap statistic. J. R. Statist. Soc. B (2001)63, Part 2, pp. 411±423

Van Houtte, C., Drouet, S., & Cotton, F. (2011). Analysis of the origins of κ (kappa) to compute hard rock to rock adjustment factors for GMPEs. Bulletin of the Seismological Society of America, 101(6), 2926-2941.

Van Houtte, C., Ktenidou, O.J., Larkin, T. and Holden, C., 2018. A continuous map of near-surface S-wave attenuation in New Zealand. Geophysical Journal International, 213(1), pp.408-425.

Wald, D. J., & Allen, T. I. (2007). Topographic Slope as a Proxy for Seismic Site Conditions and Amplification. Bull. Seismol. Soc. Am. 97(5) 1379–1395.

Wasserstein, R. L., and N. A. Lazar (2016). The ASA's statement on p-values: Context, process, and purpose, Am. Stat. 70, no. 2, 129–133.

APPENDIX I

Coefficients of ITA18-FAS

Table A1. Calibration coefficients and standard deviations of ITA18-FAS R_{JB}.

f [Hz]	a	b_1	b_2	c_1	c_2	c_3	k	f_1	f_2	τ	ϕ_{S2S}	ϕ_0
0.106	0.689	1.341	0.964	0.042	-0.712	-9.05E-05	-0.340	0.047	0.066	0.209	0.206	0.204
0.114	0.768	1.335	0.944	0.042	-0.703	-1.88E-04	-0.367	0.046	0.063	0.208	0.206	0.199
0.122	0.818	1.320	0.936	0.047	-0.687	-3.78E-04	-0.387	0.045	0.062	0.206	0.208	0.202
0.131	0.925	1.307	0.908	0.052	-0.697	-4.17E-04	-0.416	0.037	0.047	0.202	0.205	0.195
0.140	1.033	1.305	0.874	0.050	-0.714	-2.96E-04	-0.444	0.021	0.033	0.205	0.205	0.197
0.151	1.104	1.320	0.869	0.041	-0.713	-3.49E-04	-0.468	-0.032	0.022	0.215	0.209	0.200
0.162	1.188	1.328	0.824	0.032	-0.708	-4.54E-04	-0.489	-0.044	0.018	0.216	0.213	0.200
0.173	1.261	1.330	0.792	0.028	-0.704	-5.37E-04	-0.524	-0.067	0.003	0.215	0.221	0.199
0.186	1.325	1.319	0.769	0.028	-0.703	-5.86E-04	-0.546	-0.089	-0.015	0.213	0.226	0.196
0.199	1.407	1.309	0.731	0.030	-0.719	-6.05E-04	-0.569	-0.102	-0.028	0.214	0.228	0.189
0.213	1.480	1.327	0.689	0.035	-0.754	-5.68E-04	-0.581	-0.120	-0.033	0.230	0.236	0.196
0.229	1.541	1.307	0.640	0.039	-0.763	-6.30E-04	-0.604	-0.119	-0.039	0.224	0.240	0.190
0.245	1.604	1.273	0.598	0.047	-0.787	-6.47E-04	-0.625	-0.118	-0.053	0.218	0.243	0.187
0.263	1.656	1.245	0.601	0.045	-0.810	-5.26E-04	-0.635	-0.122	-0.069	0.213	0.240	0.187
0.282	1.696	1.231	0.582	0.043	-0.810	-5.14E-04	-0.643	-0.113	-0.065	0.210	0.238	0.186
0.303	1.704	1.183	0.581	0.043	-0.832	-3.67E-04	-0.656	-0.095	-0.063	0.225	0.241	0.190
0.324	1.768	1.156	0.546	0.048	-0.868	-1.73E-04	-0.691	-0.094	-0.070	0.222	0.243	0.187
0.348	1.816	1.125	0.510	0.055	-0.895	-9.12E-05	-0.714	-0.076	-0.068	0.210	0.243	0.186
0.373	1.855	1.105	0.470	0.057	-0.911	-8.84E-05	-0.745	-0.057	-0.062	0.199	0.241	0.186

0.400	1.910	1.083	0.438	0.059	-0.939	4.89E-05	-0.773	-0.051	-0.059	0.193	0.241	0.186
0.429	1.956	1.046	0.446	0.063	-0.978	2.42E-04	-0.788	-0.048	-0.067	0.181	0.242	0.186
0.460	1.990	1.022	0.419	0.070	-0.987	2.07E-04	-0.786	-0.035	-0.060	0.174	0.242	0.182
0.493	2.009	0.985	0.386	0.083	-0.996	1.76E-04	-0.791	-0.033	-0.047	0.166	0.244	0.180
0.529	2.037	0.960	0.364	0.089	-1.006	1.88E-04	-0.805	-0.040	-0.050	0.163	0.245	0.180
0.567	2.094	0.937	0.356	0.091	-1.031	2.83E-04	-0.810	-0.045	-0.055	0.160	0.242	0.180
0.608	2.121	0.909	0.367	0.093	-1.056	3.62E-04	-0.796	-0.022	-0.035	0.155	0.239	0.183
0.652	2.132	0.895	0.352	0.093	-1.054	2.89E-04	-0.785	-0.002	-0.019	0.154	0.236	0.182
0.699	2.163	0.885	0.334	0.092	-1.051	1.82E-04	-0.781	0.006	-0.020	0.152	0.232	0.182
0.749	2.189	0.865	0.324	0.094	-1.054	1.02E-04	-0.772	-0.001	-0.021	0.149	0.229	0.182
0.804	2.193	0.836	0.310	0.100	-1.052	-2.00E-05	-0.774	-0.002	-0.017	0.151	0.228	0.181
0.862	2.208	0.815	0.302	0.101	-1.054	-1.01E-04	-0.780	0.000	-0.015	0.146	0.228	0.181
0.924	2.236	0.793	0.300	0.101	-1.068	-1.25E-04	-0.769	0.004	-0.018	0.149	0.228	0.180
0.991	2.256	0.770	0.290	0.104	-1.076	-1.99E-04	-0.751	0.014	-0.011	0.152	0.227	0.180
1.062	2.300	0.746	0.287	0.105	-1.105	-1.94E-04	-0.744	0.009	-0.006	0.154	0.226	0.180
1.139	2.324	0.713	0.270	0.110	-1.117	-2.99E-04	-0.733	0.009	-0.016	0.154	0.221	0.180
1.221	2.338	0.697	0.271	0.108	-1.115	-4.39E-04	-0.729	0.011	-0.021	0.150	0.216	0.181
1.309	2.376	0.695	0.282	0.100	-1.125	-4.89E-04	-0.720	0.017	-0.020	0.151	0.216	0.180
1.404	2.392	0.679	0.271	0.102	-1.130	-5.89E-04	-0.726	0.021	-0.027	0.150	0.218	0.180
1.505	2.384	0.649	0.247	0.109	-1.129	-7.24E-04	-0.727	0.028	-0.031	0.145	0.218	0.181
1.614	2.378	0.629	0.249	0.110	-1.126	-9.08E-04	-0.717	0.036	-0.031	0.139	0.217	0.181
1.731	2.372	0.609	0.248	0.112	-1.117	-1.16E-03	-0.701	0.039	-0.028	0.132	0.216	0.182
1.856	2.366	0.588	0.229	0.118	-1.109	-1.43E-03	-0.680	0.043	-0.020	0.126	0.217	0.181
1.990	2.351	0.567	0.215	0.123	-1.097	-1.69E-03	-0.661	0.044	-0.011	0.121	0.219	0.181

2.134	2.323	0.549	0.207	0.126	-1.076	-2.00E-03	-0.637	0.047	-0.004	0.119	0.219	0.183
2.288	2.304	0.541	0.209	0.124	-1.055	-2.31E-03	-0.609	0.048	-0.004	0.120	0.220	0.182
2.453	2.301	0.532	0.211	0.122	-1.053	-2.49E-03	-0.589	0.058	-0.003	0.125	0.221	0.182
2.631	2.329	0.529	0.203	0.121	-1.065	-2.59E-03	-0.584	0.067	-0.007	0.132	0.223	0.183
2.821	2.373	0.521	0.199	0.120	-1.091	-2.67E-03	-0.563	0.063	-0.009	0.135	0.224	0.185
3.025	2.379	0.496	0.197	0.125	-1.111	-2.73E-03	-0.531	0.060	-0.005	0.134	0.228	0.185
3.243	2.385	0.484	0.194	0.125	-1.121	-2.85E-03	-0.508	0.070	0.003	0.135	0.233	0.183
3.477	2.381	0.486	0.183	0.121	-1.107	-3.16E-03	-0.473	0.080	0.008	0.139	0.239	0.181
3.729	2.357	0.473	0.171	0.123	-1.086	-3.55E-03	-0.449	0.076	0.007	0.144	0.243	0.182
3.998	2.326	0.457	0.168	0.125	-1.067	-3.89E-03	-0.427	0.065	0.007	0.146	0.249	0.183
4.287	2.312	0.449	0.156	0.125	-1.054	-4.18E-03	-0.403	0.065	0.001	0.150	0.256	0.183
4.597	2.324	0.443	0.141	0.124	-1.068	-4.34E-03	-0.381	0.076	0.003	0.153	0.263	0.183
4.929	2.319	0.431	0.148	0.124	-1.079	-4.55E-03	-0.354	0.087	0.013	0.155	0.271	0.183
5.285	2.304	0.419	0.138	0.126	-1.086	-4.81E-03	-0.337	0.098	0.020	0.158	0.280	0.186
5.667	2.283	0.408	0.130	0.127	-1.090	-4.99E-03	-0.305	0.104	0.024	0.162	0.286	0.189
6.077	2.248	0.391	0.128	0.130	-1.094	-5.19E-03	-0.271	0.113	0.030	0.168	0.289	0.189
6.516	2.222	0.367	0.122	0.135	-1.108	-5.39E-03	-0.237	0.123	0.038	0.173	0.295	0.190
6.987	2.196	0.349	0.116	0.138	-1.117	-5.62E-03	-0.200	0.131	0.044	0.178	0.303	0.192
7.491	2.176	0.345	0.112	0.137	-1.123	-5.82E-03	-0.170	0.136	0.051	0.184	0.310	0.194
8.033	2.173	0.336	0.098	0.141	-1.145	-5.95E-03	-0.143	0.140	0.048	0.189	0.319	0.193
8.613	2.178	0.319	0.086	0.147	-1.181	-6.04E-03	-0.114	0.143	0.044	0.195	0.328	0.194
9.236	2.154	0.312	0.093	0.145	-1.194	-6.21E-03	-0.088	0.141	0.055	0.198	0.337	0.197
9.903	2.114	0.307	0.097	0.142	-1.203	-6.34E-03	-0.067	0.144	0.067	0.202	0.345	0.199
10.618	2.123	0.296	0.103	0.140	-1.259	-6.15E-03	-0.047	0.148	0.073	0.208	0.348	0.202

11.386	2.127	0.289	0.118	0.137	-1.311	-6.00E-03	-0.016	0.159	0.075	0.213	0.353	0.204
12.208	2.120	0.281	0.130	0.135	-1.354	-5.90E-03	0.013	0.167	0.071	0.216	0.362	0.205
13.091	2.112	0.274	0.143	0.131	-1.396	-5.76E-03	0.026	0.165	0.065	0.219	0.371	0.210
14.037	2.099	0.282	0.163	0.121	-1.429	-5.62E-03	0.042	0.163	0.065	0.223	0.379	0.215
15.051	2.097	0.283	0.179	0.114	-1.480	-5.34E-03	0.058	0.165	0.062	0.224	0.384	0.217
16.138	2.098	0.281	0.197	0.107	-1.538	-5.01E-03	0.068	0.157	0.055	0.225	0.387	0.222
17.305	2.091	0.291	0.224	0.097	-1.585	-4.74E-03	0.065	0.146	0.051	0.227	0.389	0.230
18.555	2.096	0.315	0.249	0.082	-1.633	-4.39E-03	0.059	0.150	0.045	0.228	0.394	0.238
19.896	2.095	0.324	0.278	0.070	-1.697	-3.87E-03	0.058	0.148	0.040	0.229	0.397	0.245
21.333	2.139	0.319	0.279	0.070	-1.814	-2.75E-03	0.058	0.141	0.027	0.237	0.396	0.244
22.875	2.168	0.335	0.312	0.056	-1.898	-2.03E-03	0.049	0.129	0.023	0.240	0.400	0.251
24.528	2.163	0.356	0.340	0.042	-1.962	-1.41E-03	0.020	0.115	0.024	0.240	0.405	0.259
26.300	2.127	0.374	0.367	0.024	-2.006	-9.86E-04	-0.003	0.103	0.019	0.252	0.413	0.262
28.201	2.153	0.407	0.420	-0.004	-2.095	-1.50E-04	-0.032	0.093	0.008	0.260	0.413	0.269

Table A2. Calibration coefficients and standard deviations of ITA18-FAS R_{rup}.

f [Hz]	a	b_1	b_2	c_1	c_2	c_3	k	f_1	f_2	τ	ϕ_{S2S}	ϕ_0
0.106	0.704	1.275	0.906	0.075	-0.756	-6.94E-05	-0.339	0.051	0.074	0.202	0.206	0.204
0.114	0.784	1.270	0.887	0.075	-0.747	-1.61E-04	-0.366	0.051	0.071	0.201	0.206	0.199
0.122	0.838	1.254	0.879	0.080	-0.734	-3.34E-04	-0.386	0.050	0.070	0.199	0.207	0.202
0.131	0.941	1.241	0.851	0.085	-0.741	-3.90E-04	-0.415	0.042	0.055	0.194	0.204	0.196
0.140	1.042	1.238	0.816	0.084	-0.754	-2.97E-04	-0.444	0.026	0.042	0.196	0.204	0.198
0.151	1.111	1.254	0.816	0.073	-0.751	-3.53E-04	-0.466	-0.028	0.030	0.208	0.208	0.201
0.162	1.201	1.264	0.772	0.064	-0.749	-4.36E-04	-0.487	-0.040	0.026	0.208	0.212	0.201
0.173	1.280	1.268	0.742	0.058	-0.748	-4.97E-04	-0.522	-0.063	0.011	0.207	0.220	0.199
0.186	1.347	1.258	0.720	0.058	-0.750	-5.33E-04	-0.544	-0.084	-0.007	0.204	0.225	0.197
0.199	1.432	1.247	0.681	0.060	-0.769	-5.39E-04	-0.568	-0.097	-0.020	0.206	0.226	0.190
0.213	1.496	1.266	0.634	0.067	-0.797	-5.54E-04	-0.578	-0.115	-0.025	0.219	0.236	0.197
0.229	1.556	1.242	0.581	0.073	-0.808	-6.13E-04	-0.601	-0.113	-0.031	0.213	0.240	0.191
0.245	1.624	1.203	0.535	0.083	-0.838	-6.04E-04	-0.622	-0.112	-0.045	0.207	0.243	0.188
0.263	1.681	1.173	0.537	0.082	-0.866	-4.56E-04	-0.632	-0.116	-0.061	0.202	0.240	0.188
0.282	1.722	1.159	0.519	0.080	-0.867	-4.39E-04	-0.640	-0.107	-0.057	0.200	0.237	0.186
0.303	1.732	1.111	0.516	0.081	-0.890	-2.97E-04	-0.653	-0.092	-0.053	0.212	0.240	0.190
0.324	1.793	1.080	0.477	0.088	-0.926	-1.11E-04	-0.688	-0.091	-0.060	0.208	0.242	0.188
0.348	1.846	1.047	0.439	0.096	-0.958	-8.54E-06	-0.710	-0.073	-0.057	0.196	0.243	0.186
0.373	1.890	1.025	0.398	0.100	-0.979	1.92E-05	-0.740	-0.054	-0.052	0.185	0.241	0.187
0.400	1.950	0.998	0.360	0.104	-1.015	1.91E-04	-0.768	-0.048	-0.048	0.178	0.242	0.185
0.429	2.000	0.959	0.365	0.110	-1.057	3.92E-04	-0.783	-0.048	-0.053	0.166	0.243	0.185
0.460	2.038	0.934	0.338	0.117	-1.069	3.70E-04	-0.781	-0.035	-0.046	0.159	0.243	0.181

0.493	2.064	0.896	0.304	0.131	-1.086	3.76E-04	-0.785	-0.032	-0.035	0.151	0.245	0.180
0.529	2.092	0.871	0.284	0.136	-1.094	3.78E-04	-0.800	-0.039	-0.036	0.149	0.246	0.179
0.567	2.148	0.847	0.274	0.139	-1.119	4.69E-04	-0.804	-0.044	-0.041	0.146	0.243	0.180
0.608	2.182	0.816	0.283	0.142	-1.150	5.78E-04	-0.790	-0.022	-0.023	0.142	0.240	0.182
0.652	2.190	0.802	0.268	0.143	-1.146	4.93E-04	-0.779	-0.003	-0.007	0.142	0.236	0.181
0.699	2.209	0.793	0.251	0.141	-1.134	3.34E-04	-0.775	0.005	-0.009	0.140	0.232	0.182
0.749	2.235	0.774	0.240	0.143	-1.135	2.47E-04	-0.765	-0.002	-0.010	0.139	0.229	0.182
0.804	2.244	0.746	0.228	0.148	-1.136	1.42E-04	-0.767	-0.003	-0.005	0.143	0.228	0.181
0.862	2.261	0.723	0.218	0.149	-1.140	7.11E-05	-0.773	0.000	-0.002	0.139	0.229	0.181
0.924	2.284	0.699	0.214	0.151	-1.151	2.73E-05	-0.761	0.004	-0.005	0.142	0.228	0.180
0.991	2.304	0.675	0.203	0.154	-1.161	-4.33E-05	-0.744	0.014	0.002	0.147	0.227	0.180
1.062	2.346	0.650	0.198	0.156	-1.188	-5.07E-05	-0.736	0.010	0.007	0.149	0.227	0.180
1.139	2.364	0.615	0.179	0.162	-1.196	-1.84E-04	-0.726	0.009	-0.003	0.147	0.221	0.181
1.221	2.380	0.598	0.179	0.161	-1.196	-3.13E-04	-0.721	0.012	-0.008	0.145	0.217	0.181
1.309	2.426	0.596	0.190	0.153	-1.213	-3.27E-04	-0.712	0.018	-0.007	0.147	0.217	0.179
1.404	2.444	0.579	0.179	0.154	-1.220	-4.21E-04	-0.718	0.022	-0.013	0.147	0.218	0.180
1.505	2.433	0.549	0.154	0.163	-1.216	-5.71E-04	-0.719	0.029	-0.018	0.143	0.219	0.180
1.614	2.430	0.528	0.156	0.164	-1.215	-7.43E-04	-0.709	0.037	-0.017	0.138	0.218	0.181
1.731	2.421	0.508	0.155	0.165	-1.204	-1.01E-03	-0.693	0.041	-0.015	0.133	0.217	0.181
1.856	2.408	0.488	0.136	0.171	-1.190	-1.32E-03	-0.671	0.044	-0.007	0.128	0.217	0.181
1.990	2.387	0.470	0.125	0.174	-1.172	-1.62E-03	-0.653	0.046	0.002	0.122	0.218	0.182
2.134	2.355	0.452	0.117	0.177	-1.146	-1.95E-03	-0.628	0.049	0.008	0.121	0.218	0.184
2.288	2.333	0.444	0.119	0.175	-1.124	-2.26E-03	-0.600	0.050	0.009	0.122	0.219	0.183
2.453	2.328	0.435	0.120	0.174	-1.119	-2.45E-03	-0.581	0.060	0.010	0.129	0.220	0.184

2.631	2.351	0.431	0.110	0.173	-1.129	-2.58E-03	-0.576	0.069	0.007	0.137	0.222	0.184
2.821	2.392	0.420	0.104	0.174	-1.154	-2.67E-03	-0.554	0.065	0.004	0.141	0.224	0.187
3.025	2.402	0.391	0.099	0.181	-1.179	-2.71E-03	-0.522	0.063	0.009	0.141	0.228	0.187
3.243	2.407	0.376	0.092	0.182	-1.191	-2.83E-03	-0.499	0.073	0.017	0.141	0.233	0.185
3.477	2.406	0.377	0.081	0.179	-1.180	-3.12E-03	-0.464	0.084	0.023	0.144	0.239	0.183
3.729	2.389	0.365	0.070	0.181	-1.164	-3.49E-03	-0.440	0.079	0.022	0.149	0.243	0.183
3.998	2.357	0.350	0.068	0.182	-1.142	-3.84E-03	-0.419	0.069	0.022	0.153	0.248	0.185
4.287	2.341	0.340	0.055	0.182	-1.130	-4.13E-03	-0.395	0.069	0.017	0.157	0.255	0.184
4.597	2.347	0.333	0.037	0.183	-1.139	-4.31E-03	-0.372	0.080	0.019	0.161	0.262	0.184
4.929	2.333	0.320	0.043	0.183	-1.145	-4.57E-03	-0.345	0.091	0.030	0.164	0.271	0.185
5.285	2.320	0.305	0.031	0.187	-1.155	-4.81E-03	-0.328	0.102	0.036	0.169	0.280	0.188
5.667	2.303	0.292	0.021	0.189	-1.163	-4.98E-03	-0.295	0.109	0.041	0.173	0.286	0.191
6.077	2.266	0.273	0.018	0.192	-1.166	-5.19E-03	-0.262	0.118	0.048	0.180	0.289	0.191
6.516	2.237	0.247	0.009	0.199	-1.181	-5.39E-03	-0.227	0.129	0.057	0.186	0.294	0.192
6.987	2.206	0.227	0.002	0.203	-1.185	-5.65E-03	-0.190	0.137	0.063	0.190	0.302	0.194
7.491	2.183	0.222	-0.003	0.203	-1.191	-5.87E-03	-0.160	0.141	0.071	0.196	0.310	0.196
8.033	2.188	0.211	-0.019	0.208	-1.219	-5.97E-03	-0.133	0.145	0.068	0.201	0.319	0.195
8.613	2.196	0.189	-0.035	0.217	-1.261	-6.04E-03	-0.104	0.148	0.065	0.208	0.327	0.196
9.236	2.169	0.181	-0.029	0.215	-1.272	-6.23E-03	-0.078	0.147	0.077	0.213	0.336	0.199
9.903	2.131	0.175	-0.026	0.213	-1.283	-6.35E-03	-0.057	0.150	0.089	0.217	0.344	0.202
10.618	2.139	0.160	-0.024	0.214	-1.341	-6.17E-03	-0.037	0.154	0.096	0.223	0.347	0.204
11.386	2.137	0.149	-0.013	0.212	-1.389	-6.04E-03	-0.006	0.164	0.098	0.229	0.352	0.207
12.208	2.127	0.138	-0.003	0.211	-1.431	-5.96E-03	0.024	0.173	0.095	0.234	0.361	0.209
13.091	2.123	0.128	0.008	0.209	-1.479	-5.80E-03	0.036	0.170	0.090	0.238	0.371	0.213

14.037	2.109	0.133	0.024	0.201	-1.513	-5.66E-03	0.052	0.169	0.090	0.241	0.378	0.219
15.051	2.101	0.133	0.038	0.195	-1.561	-5.41E-03	0.069	0.171	0.088	0.243	0.383	0.222
16.138	2.103	0.126	0.053	0.191	-1.622	-5.07E-03	0.078	0.163	0.082	0.245	0.386	0.226
17.305	2.097	0.132	0.076	0.183	-1.672	-4.79E-03	0.075	0.152	0.078	0.248	0.388	0.234
18.555	2.098	0.152	0.098	0.170	-1.719	-4.46E-03	0.070	0.154	0.072	0.249	0.393	0.242
19.896	2.093	0.159	0.126	0.159	-1.780	-3.97E-03	0.069	0.152	0.066	0.250	0.396	0.250
21.333	2.132	0.144	0.120	0.165	-1.899	-2.86E-03	0.068	0.141	0.049	0.258	0.395	0.249
22.875	2.157	0.157	0.149	0.153	-1.982	-2.17E-03	0.060	0.127	0.045	0.261	0.400	0.256
24.528	2.147	0.175	0.176	0.140	-2.042	-1.57E-03	0.031	0.110	0.045	0.259	0.405	0.266
26.300	2.092	0.184	0.200	0.126	-2.076	-1.23E-03	0.010	0.096	0.037	0.269	0.413	0.269
28.201	2.165	0.212	0.232	0.103	-2.198	-2.18E-04	-0.020	0.088	0.022	0.268	0.415	0.275

APPENDIX II

Plots of ITA18 FAS
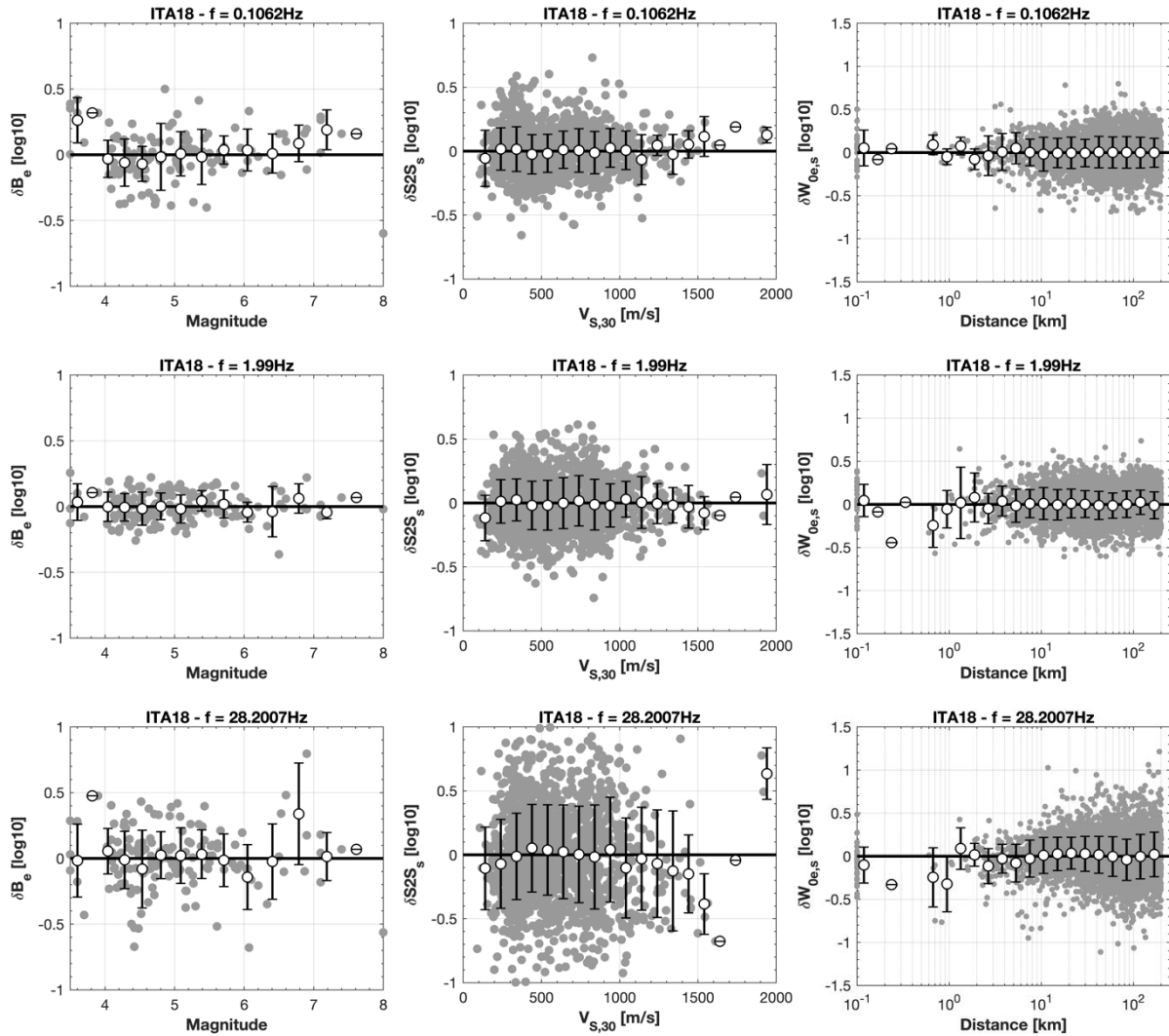
Figure B1. Residual terms of ITA18 FAS model in R_{JB}. Left: between-event vs. magnitude; middle: site-to-site vs. $V_{S,30}$; right: event- and site- corrected residual vs. distance. Top: f=0.1Hz; middle: f=2Hz; bottom: f=28Hz.
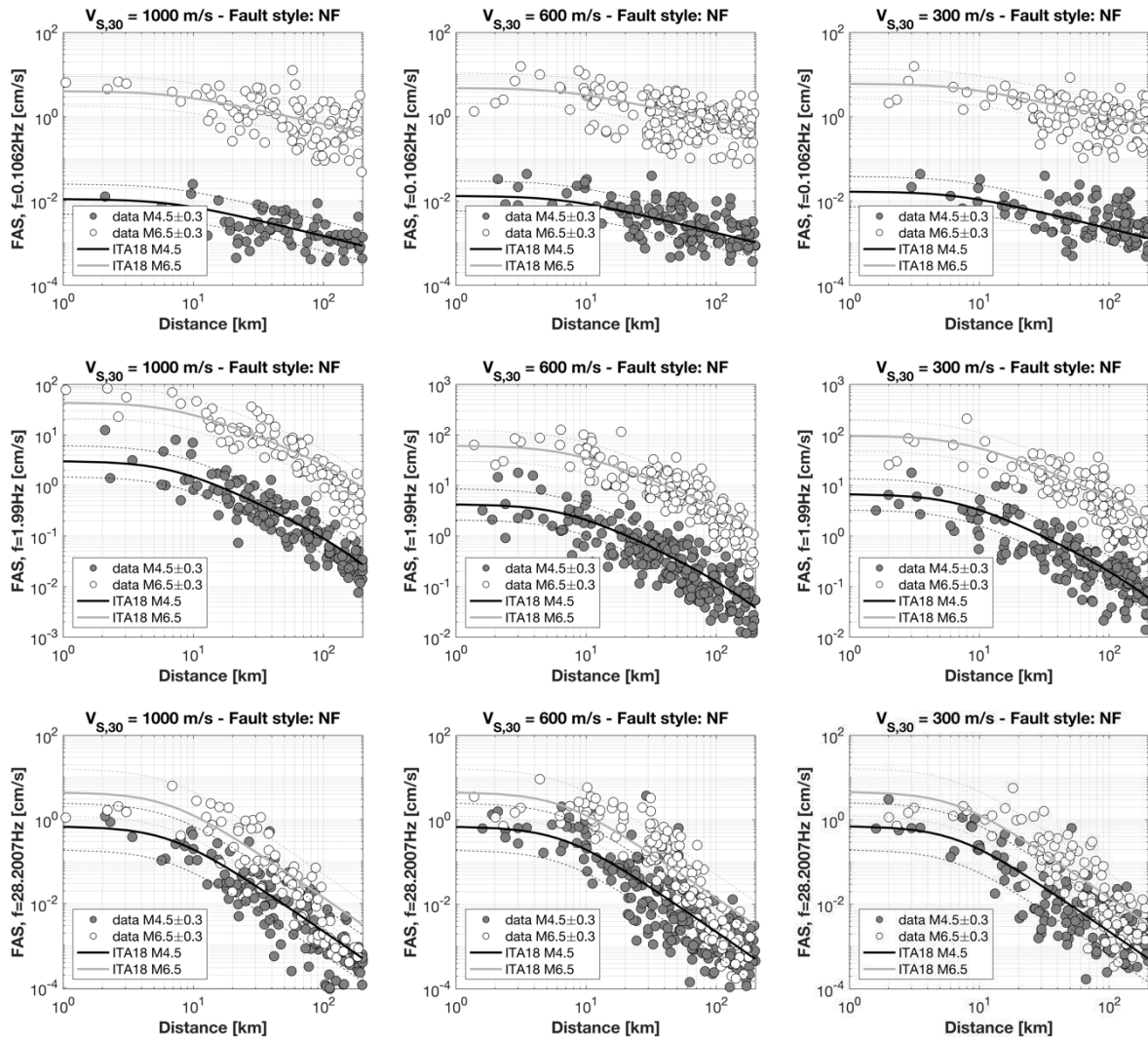
Figure B2. Distance dependent attenuation of ITA18 FAS model in R_{JB}. Left: $V_{S,30}$=1000m/s; middle: $V_{S,30}$=600m/s; right: $V_{S,30}$=300m/s. Top: f=0.1Hz; middle: f=2Hz; bottom: f=28Hz.

APPENDIX III

List of the candidate stations belonging to cluster #8 and #2 and the corresponding ranking

Table C1. List of the cluster #8 stations with "Final score" ≥ 4.75. For each station, the table reports: network code (NET CODE); station code (STA CODE); weight for cluster #1 (δS2S score); housing/proximity condition (HOU); housing score (HOU score); scale of the geological/lithological/litothecnical map (GEO scale); EC8 subsoil classification from surface geology (EC8 GEO); weight for the geological proxy (GEO score); slope value (TOP); topographic weight (TOP score); $V_{S,30}$ value (VS30); $V_{S,30}$ estimation method (VS30 method); VS30 weight (VS30 score); shape of H/V curve (HV); H/V analysis (HV type); weight for the H/V proxy (HV score); number of available proxies (Av proxies). FF = free-field condition; CAB = Electrical transformation cabin; NO-FF = no free-field condition; F = flat curve; BB = broad-band curve; P = picked curve; Meas = measured by geophysical test; Topog = inferred from topographic proxy

NET CODE	STA CODE	δS2S score	HOU	HOU score	GEO scale	EC8 GEO	GEO score	TOP	TOP score	VS30 [m/s]	VS30 method	VS30 score	HV	HV type	HV score	Av. proxies	Final score
IT	MND	1.00	FF	0.500	10000	A	2.0	1.0	0.50	800	Meas	0.767	HVNSR	F	2.0	6	7.53
IT	PPL1	1.00	FF	0.500	10000	A	2.0	0.6	0.50	775	Meas	0.758	HVNSR	F	2.0	6	7.52
IT	SDG	0.75	FF	0.500	10000	A	2.0	0.8	0.50	800	Meas	0.767	HVNSR	F	2.0	6	7.28
IT	MNF	1.00	NO-FF	0.000	10000	A	2.0	16.4	0.25	1060	Meas	0.853	HVNSR	F	2.0	6	6.96
IT	BBN	0.75	FF	0.500	100000	A	1.5	9.5	0.50	1000	Meas	0.833	HVNSR	F	2.0	6	6.92
IT	SBC	1.00	FF	0.500	10000	A	2.0	10.9	0.50	1298	Meas	0.933	HVSR-S	F	1.0	6	6.87
IT	MZZ	1.00	FF	0.500	10000	A	2.0	9.3	0.50	794	Topo	0.765	HVNSR	F	2.0	6	6.76
IT	MVB	1.00	FF	0.500	5000	B	1.0	3.6	0.50	1046	Meas	0.849	HVNSR	F	2.0	6	6.70
IV	ATVO	1.00	FF	0.500	10000	B	1.0	8.6	0.50	1033	Meas	0.844	HVNSR	F	2.0	6	6.69
IT	SCN	1.00	FF	0.500	5000	A	2.0	10.4	0.50	839	Meas	0.780	HVNSR	BB	1.0	6	6.56
IT	LSP	0.75	FF	0.500	10000	A	2.0	12.8	0.50	886	Topo	0.795	HVNSR	F	2.0	6	6.55
IV	ATLO	1.00	FF	0.500	10000	B	1.0	3.3	0.50	767	Meas	0.756	HVNSR	F	2.0	6	6.51
IT	LSS	1.00	FF	0.500	10000	B	1.0	25.9	0.25	1091	Meas	0.864	HVNSR	F	2.0	6	6.48
IT	RNC	1.00	CAB	0.375	10000	B	1.0	14.1	0.50	859	Meas	0.786	HVNSR	F	2.0	6	6.45
IT	NRN	1.00	CAB	0.375	10000	A	2.0	13.6	0.50	812	Meas	0.771	HVNSR	BB	1.0	6	6.42

Lanzano G., Felicetta C., Pacor F. - Metodology to identify reference rock sites - SIGMA2-XXXX-YY-ZZ

IT	BGR	0.75	FF	0.500	5000	B	1.0	10.2	0.50	829	Meas	0.776	HVNSR	F	2.0	6	6.30
IT	SVA	1.00	FF	0.500	100000	A	1.5	11.3	0.50	846	Topo	0.782	HVNSR	F	2.0	6	6.28
IV	MCEL	1.00	FF	0.500	100000	A	1.5	10.1	0.50	815	Topo	0.772	HVNSR	F	2.0	6	6.27
IT	SUL	1.00	FF	0.500	100000	A	1.5	26.1	0.25	1265	Topo	0.922	HVSR-C	F	2.0	6	6.17
MN	CUC	1.00	FF	0.500	100000	A	1.5	17.6	0.25	1016	Topo	0.839	HVNSR	F	2.0	6	6.09
IV	FIAM	1.00	FF	0.500	100000	A	1.5	17.3	0.25	1007	Topo	0.836	HVNSR	F	2.0	6	6.09
IV	T1256	0.75		0.000	10000	A	2.0	7.9	0.50	757	Topo	0.752	HVNSR	F	2.0	5	6.00
IT	VRL	1.00	FF	0.500	25000	A	1.5	17.6	0.25	855	Meas	0.785	HVRS	F	1.0	6	5.82
IV	T1215	0.75		0.000	10000	A	2.0	15.3	0.25	951	Topo	0.817	HVNSR	F	2.0	5	5.82
IV	RM27	1.00		0.000	100000	A	1.5	10.9	0.50	836	Topo	0.779	HVSR-C	F	2.0	5	5.78
IT	FMG	1.00	NO-FF	0.000	5000	B	1.0	17.4	0.25	790	Meas	0.763	HVNSR	F	2.0	6	5.78
IT	SLO	1.00	FF	0.500	10000	B	1.0	10.4	0.50	823	Topo	0.774	HVSR-C	F	2.0	6	5.77
IV	T1217	1.00	FF	0.500	10000	B	1.0	9.0	0.50	786	Topo	0.762	HVNSR	F	2.0	6	5.76
IT	DCM	1.00	FF	0.500	100000	C	0.0	1.3	0.50	1000	Meas	0.833	HVNSR	F	2.0	6	5.67
IT	PAN	1.00	FF	0.500	10000	B	1.0	12.2	0.50	977	Meas	0.826	HVSR-S	F	1.0	6	5.65
IT	CVM	0.75	NO-FF	0.000	100000	A	1.5	13.0	0.50	891	Topo	0.797	HVNSR	F	2.0	6	5.55
IV	BSSO	0.75	FF	0.500	100000	A	1.5	6.3	0.50	659	Topo	0.296	HVNSR	F	2.0	6	5.55
IT	CAR	1.00	FF	0.500	100000	A	1.5	1.4	0.50	387	Topo	0.000	HVNSR	F	2.0	6	5.50
IT	MNT	1.00	NO-FF	0.000	10000	A	2.0	5.1	0.50	590	Topo	0.000	HVNSR	F	2.0	6	5.50
IT	GRN	1.00	CAB	0.375	5000	B	1.0	17.6	0.25	1015	Topo	0.838	HVNSR	F	2.0	6	5.46
IT	PSC	1.00	FF	0.500	5000	A	2.0	19.5	0.25	1000	Meas	0.833	HVNSR	P	0.0	6	5.42
IV	MRLC	0.75		0.000	100000	A	1.5	10.7	0.50	861	Meas	0.787	HVNSR	BB	1.0	5	5.32
IV	FIU1	0.75	NO-FF	0.000	10000	A	2.0	5.5	0.50	612	Topo	0.059	HVNSR	F	2.0	6	5.31
IT	MMP1	0.75	FF	0.500	5000	A	2.0	13.6	0.50	800	Meas	0.767	HVNSR	P	0.0	6	5.28
IV	SERS	1.00	FF	0.500	100000	B	0.5	10.9	0.50	837	Topo	0.779	HVNSR	F	2.0	6	5.28
IV	ASQU	1.00	FF	0.500	100000	B	0.5	10.8	0.50	833	Topo	0.778	HVNSR	F	2.0	6	5.28

IV	GUAR	1.00	FF	0.500	100000	A	1.5	9.2	0.50	791	Topo	0.764	HVSR-S	F	1.0	6	5.26
IV	RM01	1.00	FF	0.500	100000	A	1.5	9.1	0.50	790	Topo	0.763	HVSR-C	BB	1.0	6	5.26
IV	ATPI	1.00	FF	0.500	100000	B	0.5	8.0	0.50	762	Topo	0.754	HVNSR	F	2.0	6	5.25
IV	PIGN	0.75	FF	0.500	100000	A	1.5	4.4	0.50	560	Topo	0.000	HVNSR	F	2.0	6	5.25
IV	POFI	0.75	FF	0.500	100000	A	1.5	2.2	0.50	443	Topo	0.000	HVNSR	F	2.0	6	5.25
IV	RM03	0.75	FF	0.500	100000	A	1.5	3.5	0.50	517	Topo	0.000	HVSR-C	F	2.0	6	5.25
IV	SACR	0.75	FF	0.500	100000	A	1.5	3.1	0.50	501	Topo	0.000	HVNSR	F	2.0	6	5.25
MN	VLC	0.75	FF	0.500	100000	A	1.5	2.6	0.50	469	Topo	0.000	HVNSR	F	2.0	6	5.25
IV	CAFI	1.00	FF	0.500	100000	B	0.5	7.6	0.50	738	Topo	0.690	HVNSR	F	2.0	6	5.19
IV	SACS	0.75	FF	0.500	100000	B	0.5	1.1	0.50	692	Meas	0.461	HVNSR	F	2.0	6	5.17
IT	CDS	1.00	FF	0.500	100000	B	0.5	25.9	0.25	1259	Topo	0.920	HVNSR	F	2.0	6	5.17
IT	AME	1.00	NO-FF	0.000	10000	A	2.0	25.2	0.25	1236	Topo	0.912	HVRS	F	1.0	6	5.16
IV	SNTG	1.00	NO-FF	0.000	10000	B	1.0	21.6	0.25	1130	Topo	0.877	HVNSR	F	2.0	6	5.13
IV	T0106	1.00	FF	0.500	100000	A	1.5	19.2	0.25	1061	Topo	0.854	HVSR-C	BB	1.0	6	5.10
IV	FOSV	1.00	NO-FF	0.000	10000	B	1.0	17.3	0.25	1008	Topo	0.836	HVNSR	F	2.0	6	5.09
IV	SFI	1.00	FF	0.500	100000	B	0.5	17.2	0.25	1004	Topo	0.835	HVNSR	F	2.0	6	5.08
IT	FLT	1.00	FF	0.500	100000	B	0.5	16.8	0.25	993	Topo	0.831	HVNSR	F	2.0	6	5.08
IT	FRE	1.00	FF	0.500	100000	B	0.5	16.4	0.25	982	Topo	0.827	HVSR-C	F	2.0	6	5.08
IV	MML1	1.00	FF	0.500	10000	B	1.0	5.6	0.50	615	Topo	0.073	HVNSR	F	2.0	6	5.07
IT	CMB	0.75	FF	0.500	100000	B	0.5	10.9	0.50	837	Topo	0.779	HVNSR	F	2.0	6	5.03
MN	TUE	0.75	FF	0.500	100000	A	1.5	9.5	0.50	799	Topo	0.766	HVRS	F	1.0	6	5.02
IT	ORC	1.00	NO-FF	0.000	5000	B	1.0	3.0	0.50	767	Meas	0.756	HVSR-C	BB	1.0	6	5.01
XO	MN04	0.75	FF	0.500	100000	B	0.5	8.1	0.50	763	Topo	0.754	HVNSR	F	2.0	6	5.00
IT	SNO	1.00	FF	0.500	10000	B	1.0	2.0	0.50	429	Topo	0.000	HVNSR	F	2.0	6	5.00
IV	T1241	1.00	FF	0.500	10000	B	1.0	4.4	0.50	559	Topo	0.000	HVNSR	F	2.0	6	5.00
IT	TRV	0.75	CAB	0.375	100000	B	0.5	14.3	0.50	924	Topo	0.808	HVNSR	F	2.0	6	4.93

NET CODE	STA CODE	δS2S score	HOU	HOU score	GEO scale	EC8 GEO	GEO score	TOP	TOP score	VS30 [m/s]	VS30 method	VS30 score	HV	HV type	HV score	Av. proxies	Final score
IT	PLT	0.75	CAB	0.375	100000	B	0.5	11.3	0.50	847	Topo	0.782	HVNSR	F	2.0	6	4.91
MN	TIP	0.75	FF	0.500	100000	B	0.5	24.3	0.25	1208	Topo	0.903	HVNSR	F	2.0	6	4.90
IT	ANT	0.75	NO-FF	0.000	5000	A	2.0	13.1	0.50	912	Meas	0.804	HVNSR	P	0.0	6	4.86
IT	CSO1	0.75	FF	0.500	100000	B	0.5	18.8	0.25	1049	Topo	0.850	HVNSR	F	2.0	6	4.85
IT	GLT	1.00	NO-FF	0.000	10000	A	2.0	6.5	0.50	669	Topo	0.343	HVSR-S	F	1.0	6	4.84
IV	GATE	0.75	FF	0.500	100000	B	0.5	17.9	0.25	1025	Topo	0.842	HVNSR	F	2.0	6	4.84
IV	ARVD	0.75	FF	0.500	100000	A	1.5	15.6	0.25	959	Topo	0.820	HVSR-S	F	1.0	6	4.82
IT	BOI	1.00	NO-FF	0.000	100000	B	0.5	12.2	0.50	871	Topo	0.790	HVNSR	F	2.0	6	4.79
IT	BZZ	1.00	FF	0.500	100000	C	0.0	1.0	0.50	679	Meas	0.395	HVNSR	F	2.0	6	4.79
IV	MTSN	1.00	FF	0.500	100000	A	1.5	11.1	0.50	842	Topo	0.781	HVSR-S	BB	0.5	6	4.78
IT	ATN	1.00	NO-FF	0.000	100000	A	1.5	9.6	0.50	801	Topo	0.767	HVSR-S	F	1.0	6	4.77
IT	BCN	1.00	FF	0.500	100000	C	0.0	7.8	0.50	751	Topo	0.750	HVNSR	F	2.0	6	4.75
3A	MZ31	0.75	FF	0.500	5000	B	1.0	5.2	0.50	597	Topo	0.000	HVNSR	F	2.0	6	4.75
IV	SGTA	0.75		0.000	100000	A	1.5	7.0	0.50	400	Meas	0.000	HVNSR	F	2.0	5	4.75

Table C2. List of the cluster #2 stations with "Final score" ≥ 4.75. For each station, the table reports: network code (NET CODE); station code (STA CODE); weight for cluster #1 (δS2S score); housing/proximity condition (HOU); housing score (HOU score); scale of the geological/lithological/litothecnical map (GEO scale); EC8 subsoil classification from surface geology (EC8 GEO); weight for the geological proxy (GEO score); slope value (TOP); topographic weight (TOP score); $V_{S,30}$ value (VS30); $V_{S,30}$ estimation method (VS30 method); VS30 weight (VS30 score); shape of H/V curve (HV); H/V analysis (HV type); weight for the H/V proxy (HV score); number of available proxies (Av proxies). FF = free-field condition; CAB = Electrical transformation cabin; NO-FF = no free-field condition; F = flat curve; BB = broad-band curve; P = picked curve; Meas = measured by geophysical test; Topog = inferred from topographic proxy.

NET CODE	STA CODE	δS2S score	HOU	HOU score	GEO scale	EC8 GEO	GEO score	TOP	TOP score	VS30 [m/s]	VS30 method	VS30 score	HV	HV type	HV score	Av. proxies	Final score
IT	SRC	0.75	FF	0.5	10000	A	2	4.6	0.5	923	Meas	0.808	HVNSR	F	2	6	7.37
IT	BNO	0.5	FF	0.5	10000	A	2	12.3	0.5	1296	Meas	0.932	HVNSR	F	2	6	7.36
IT	LNT	0.75	FF	0.5	10000	A	2	3.5	0.5	867	Meas	0.789	HVNSR	F	2	6	7.33
IV	TERO	0.75	FF	0.5	5000	A	2	16.9	0.25	912	Meas	0.804	HVNSR	F	2	6	7.11

Lanzano G., Felicetta C., Pacor F. - Metodology to identify reference rock sites - SIGMA2-XXXX-YY-ZZ

IT	MNN	0.5	FF	0.5	10000	A	2	1.2	0.5	815	Meas	0.772	HVNSR	F	2	6	7.04
IT	VSD	0.75	NO-FF	0	10000	A	2	8.5	0.5	800	Meas	0.767	HVNSR	F	2	6	6.78
IT	CME	0.75	FF	0.5	10000	A	2	9.1	0.5	789	Topo	0.763	HVSR-C	F	2	6	6.51
IT	RGS	0.75	FF	0.5	10000	B	1	2.2	0.5	1071	Meas	0.857	HVNSR	F	2	6	6.46
IT	GNV	0.75	FF	0.5	25000	B	0.5	6.9	0.5	1152	Meas	0.884	HVNSR	F	2	6	6.02
IT	NTE	0.75	FF	0.5	100000	A	1.5	5.7	0.5	659	Meas	0.295	HVNSR	F	2	6	5.84
IV	PIEI	0.5	NO-FF	0	10000	A	2	11.0	0.5	838	Topo	0.779	HVNSR	F	2	6	5.78
IT	GNU	0.75	FF	0.5	10000	A	2	14.4	0.5	928	Topo	0.809	HVSR-C	BB	1	6	5.56
3A	MZ19	0.75	FF	0.5	5000	B	1	17.2	0.25	1005	Topo	0.835	HVNSR	F	2	6	5.33
IT	SGV	0.75	FF	0.5	5000	A	2	8.2	0.5	872	Meas	0.791	HVNSR	P	0	6	5.33
IV	BOTT	0.5		0	100000	A	1.5	14.4	0.5	927	Topo	0.809	HVSR-C	F	2	5	5.31
IT	MTC	0.5	NO-FF	0	5000	B	1	20.6	0.25	827	Meas	0.776	HVNSR	F	2	6	5.30
IV	T1211	0.75	FF	0.5	100000	A	1.5	2.6	0.5	468	Topo	0.000	HVNSR	F	2	6	5.25
IV	T1212	0.75	FF	0.5	100000	A	1.5	3.9	0.5	539	Topo	0.000	HVNSR	F	2	6	5.25
IT	GBB	0.75	CAB	0.375	10000	B	1	19.4	0.25	1066	Topo	0.855	HVSR-C	F	2	6	5.23
IT	PTL	0.75	CAB	0.375	10000	B	1	7.3	0.5	717	Topo	0.585	HVNSR	F	2	6	5.21
IT	AMT	0.5	FF	0.5	5000	B	1	4.7	0.5	670	Meas	0.350	HVNSR	F	2	6	5.20
IT	RNS	0.5	FF	0.5	20000	B	0.5	10.1	0.5	709	Meas	0.545	HVNSR	F	2	6	5.09
IV	MSRU	0.75	FF	0.5	100000	B	0.5	11.5	0.5	851	Topo	0.784	HVNSR	F	2	6	5.03
IV	CESI	0.75	FF	0.5	100000	B	0.5	11.2	0.5	844	Topo	0.781	HVNSR	F	2	6	5.03
IV	T1214	0.75		0	10000	B	1	8.2	0.5	766	Topo	0.755	HVNSR	F	2	5	5.01
IT	VGG	0.5	FF	0.5	100000	A	1.5	3.8	0.5	533	Topo	0.000	HVNSR	F	2	6	5.00
IT	CSC	0.75	NO-FF	0	10000	B	1	18.5	0.25	698	Meas	0.490	HVNSR	F	2	6	4.98
IT	COR	0.75	CAB	0.375	100000	B	0.5	9.6	0.5	803	Topo	0.768	HVNSR	F	2	6	4.89
IT	SDM	0.5	CAB	0.375	5000	C	0	7.0	0.5	752	Meas	0.751	HVNSR	F	2	6	4.88
IT	ASS	0.75	NO-FF	0	10000	A	2	18.9	0.25	1051	Topo	0.850	HVNSR	BB	1	6	4.85

Lanzano G., Felicetta C., Pacor F. - Metodology to identify reference rock sites - SIGMA2-XXXX-YY-ZZ

IV	T1244	0.5	FF	0	10000	B	1	14.0	0.5	918	Topo	0.806	HVNSR	F	2	6	4.81
IT	BRB	0.5	FF	0.5	100000	B	0.5	11.6	0.5	854	Topo	0.785	HVNSR	F	2	6	4.78
IT	CRI	0.5	FF	0.5	100000	B	0.5	10.4	0.5	824	Topo	0.775	HVNSR	F	2	6	4.77
IV	JOPP	0.5	FF	0.5	100000	B	0.5	10.3	0.5	821	Topo	0.774	HVNSR	F	2	6	4.77
IV	MOMA	0.75	FF	0.5	10000	A	2	4.9	0.5	581	Topo	0.000	HVNSR	BB	1	6	4.75

APPENDIX IV

Correction terms to scale GMMs to reference rock sites

Table D1. Correction terms to scale GMMs to reference rock sites for ITA18-SA.

T	δ	σ_δ	V_{ref}	δ_{red}	$\sigma_{\delta,red}$	a_κ	b_κ	c_κ	σ_{model}
[s]	[log₁₀]	[log₁₀]	[m/s]	[log₁₀]	[log₁₀]				[log₁₀]
0	-0.180	0.329	2285.841	-0.327	0.254	-0.190	0.324	-4.946	0.238
0.01	-0.180	0.329	2290.728	-0.327	0.254	-0.189	0.324	-4.994	0.238
0.025	-0.176	0.333	2316.878	-0.325	0.259	-0.160	0.329	-5.947	0.238
0.04	-0.175	0.349	2589.127	-0.327	0.274	-0.120	0.331	-7.476	0.246
0.05	-0.178	0.357	2886.952	-0.331	0.283	-0.099	0.303	-8.408	0.252
0.07	-0.189	0.373	3836.695	-0.354	0.293	-0.096	0.244	-9.363	0.258
0.1	-0.208	0.374	4772.035	-0.388	0.278	-0.146	0.154	-8.782	0.248
0.15	-0.200	0.372	3356.976	-0.364	0.287	-0.222	0.287	-5.116	0.273
0.2	-0.208	0.360	2848.404	-0.358	0.274	-0.237	0.241	-4.361	0.263
0.25	-0.189	0.352	2213.260	-0.343	0.262	-0.255	0.236	-3.159	0.255
0.3	-0.173	0.336	1845.968	-0.306	0.262	-0.254	0.418	-1.842	0.253
0.35	-0.163	0.316	1619.198	-0.261	0.259	-0.259	0.515	0	0.250
0.4	-0.157	0.304	1530.801	-0.230	0.257	-0.228	0.536	0	0.247
0.45	-0.148	0.293	1421.741	-0.207	0.256	-0.205	0.525	0	0.246
0.5	-0.139	0.293	1343.558	-0.194	0.255	-0.192	0.457	0	0.248
0.6	-0.140	0.286	1312.540	-0.168	0.260	-0.167	0.475	0	0.253
0.7	-0.128	0.275	1236.476	-0.147	0.246	-0.146	0.385	0	0.241
0.75	-0.124	0.272	1220.562	-0.136	0.248	-0.135	0.346	0	0.243

Lanzano G., Felicetta C., Pacor F. - Metodology to identify reference rock sites - SIGMA2-XXXX-YY-ZZ

0.8	-0.116	0.274	1185.338	-0.127	0.256	-0.126	0.307	0	0.252
0.9	-0.107	0.263	1143.413	-0.110	0.247	-0.109	0.293	0	0.244
1	-0.098	0.254	1104.716	-0.107	0.239	-0.106	0.256	0	0.236
1.2	-0.097	0.249	1090.519	-0.111	0.251	-0.109	0.351	0	0.246
1.4	-0.084	0.247	1041.469	-0.090	0.241	-0.088	0.325	0	0.237
1.6	-0.081	0.247	1029.107	-0.085	0.240	-0.083	0.253	0	0.237
1.8	-0.081	0.245	1024.194	-0.089	0.235	-0.088	0.187	0	0.233
2	-0.076	0.247	1012.441	-0.087	0.231	-0.087	0.150	0	0.230
2.5	-0.064	0.242	979.408	-0.074	0.224	-0.074	0.046	0	0.223
3	-0.055	0.250	962.273	-0.051	0.246	-0.051	0.105	0	0.245
3.5	-0.049	0.256	949.518	-0.043	0.257	-0.043	0.065	0	0.256
4	-0.043	0.263	933.635	-0.030	0.261	-0.030	0.049	0	0.260
4.5	-0.040	0.269	927.984	-0.028	0.266	-0.028	0.043	0	0.265
5	-0.037	0.269	923.755	-0.027	0.267	-0.027	0.047	0	0.266
6	-0.051	0.244	987.781	-0.051	0.245	-0.051	-0.060	0	0.244
7	-0.065	0.228	1059.955	-0.054	0.224	-0.054	-0.029	0	0.223
8	-0.068	0.224	1091.288	-0.061	0.218	-0.061	0.035	0	0.217
9	-0.066	0.225	1080.716	-0.062	0.214	-0.062	0.050	0	0.213
10	-0.069	0.225	1108.823	-0.069	0.211	-0.069	0.094	0	0.210

Table D2. Correction terms to scale GMMs to reference rock sites for ITA18-FAS.

f	δ	σ_δ	δ_{red}	$\sigma_{\delta,red}$	a_κ	b_κ	c_κ	σ_{model}
[Hz]	[log10]	[log10]	[log10]	[log10]				[log10]

Lanzano G., Felicetta C., Pacor F. - Metodology to identify reference rock sites - SIGMA2-XXXX-YY-ZZ

0.106	-0.028	0.303	0.012	0.281	0.014	0.010	0	0.276
0.114	-0.030	0.290	0.011	0.275	0.013	0.015	0	0.269
0.122	-0.032	0.282	0.013	0.265	0.016	0.022	0	0.259
0.131	-0.047	0.274	-0.008	0.260	-0.012	-0.026	0	0.255
0.140	-0.051	0.274	-0.014	0.253	-0.019	-0.039	0	0.249
0.151	-0.038	0.285	-0.011	0.266	0.012	0.131	0	0.259
0.162	-0.034	0.294	-0.004	0.279	0.035	0.222	0	0.267
0.173	-0.026	0.297	0.007	0.281	0.050	0.251	0	0.265
0.186	-0.022	0.293	0.005	0.271	0.016	0.063	0	0.262
0.199	-0.024	0.296	-0.003	0.273	0.002	0.026	0	0.267
0.213	-0.012	0.324	0.031	0.298	0.032	0.006	0	0.293
0.229	-0.015	0.319	0.033	0.294	0.025	-0.051	0	0.288
0.245	-0.016	0.308	0.034	0.288	0.016	-0.121	0	0.282
0.263	-0.023	0.300	0.025	0.289	0.041	0.091	0	0.285
0.282	-0.039	0.297	0.008	0.291	0.025	0.106	0	0.287
0.303	-0.037	0.300	0.003	0.298	-0.009	-0.087	0	0.294
0.324	-0.038	0.293	-0.005	0.281	-0.020	-0.110	0	0.276
0.348	-0.046	0.282	-0.012	0.263	-0.027	-0.099	0	0.258
0.373	-0.057	0.276	-0.026	0.254	-0.030	-0.050	0	0.248
0.400	-0.064	0.266	-0.042	0.241	-0.049	-0.090	0	0.235
0.429	-0.059	0.256	-0.041	0.227	-0.040	0.011	0	0.221
0.460	-0.064	0.256	-0.040	0.220	-0.043	-0.049	0	0.213
0.493	-0.069	0.253	-0.045	0.224	-0.048	-0.033	0	0.219
0.529	-0.075	0.250	-0.052	0.224	-0.051	0.014	0	0.221

0.567	-0.080	0.247	-0.058	0.228	-0.053	0.075	0	0.225
0.608	-0.072	0.253	-0.052	0.238	-0.052	-0.010	0	0.235
0.652	-0.069	0.252	-0.046	0.235	-0.046	-0.004	0	0.233
0.699	-0.071	0.246	-0.054	0.228	-0.051	0.059	0	0.226
0.749	-0.076	0.242	-0.059	0.235	-0.043	0.376	0	0.224
0.804	-0.082	0.239	-0.075	0.240	-0.062	0.193	0	0.233
0.862	-0.086	0.239	-0.081	0.232	-0.069	0.175	0	0.224
0.924	-0.091	0.240	-0.085	0.228	-0.079	0.101	0	0.222
0.991	-0.097	0.242	-0.083	0.222	-0.081	0.031	0	0.216
1.062	-0.099	0.248	-0.077	0.226	-0.076	0.258	0	0.209
1.139	-0.104	0.259	-0.081	0.244	-0.080	0.276	0	0.222
1.221	-0.112	0.265	-0.094	0.250	-0.093	0.283	0	0.229
1.309	-0.119	0.261	-0.105	0.238	-0.104	0.289	0	0.222
1.404	-0.124	0.264	-0.118	0.238	-0.116	0.387	0	0.224
1.505	-0.129	0.272	-0.124	0.247	-0.122	0.460	0	0.233
1.614	-0.135	0.275	-0.132	0.255	-0.130	0.508	0	0.239
1.731	-0.138	0.278	-0.147	0.248	-0.145	0.429	0	0.237
1.856	-0.137	0.284	-0.160	0.251	-0.159	0.331	0	0.242
1.990	-0.137	0.287	-0.167	0.249	-0.165	0.403	0	0.239
2.134	-0.142	0.285	-0.175	0.246	-0.172	0.493	0	0.234
2.288	-0.152	0.287	-0.187	0.248	-0.184	0.547	0	0.234
2.453	-0.158	0.289	-0.208	0.247	-0.206	0.586	0	0.232
2.631	-0.163	0.291	-0.230	0.245	-0.227	0.541	0	0.232
2.821	-0.163	0.296	-0.245	0.238	-0.243	0.517	0	0.228

3.025	-0.166	0.306	-0.263	0.238	-0.229	0.472	-1.164	0.228
3.243	-0.168	0.320	-0.283	0.241	-0.210	0.330	-2.619	0.232
3.477	-0.179	0.330	-0.313	0.241	-0.247	0.274	-2.348	0.235
3.729	-0.191	0.336	-0.334	0.240	-0.281	0.221	-1.894	0.235
3.998	-0.194	0.341	-0.344	0.236	-0.274	0.140	-2.500	0.232
4.287	-0.200	0.346	-0.346	0.239	-0.241	0.053	-3.813	0.232
4.597	-0.208	0.346	-0.350	0.241	-0.233	0.069	-4.230	0.233
4.929	-0.215	0.346	-0.357	0.244	-0.241	0.099	-4.191	0.236
5.285	-0.212	0.356	-0.362	0.253	-0.228	0.119	-4.632	0.243
5.667	-0.208	0.366	-0.359	0.266	-0.197	0.120	-5.687	0.253
6.077	-0.203	0.370	-0.353	0.274	-0.184	0.168	-5.853	0.260
6.516	-0.200	0.369	-0.358	0.267	-0.197	0.159	-5.568	0.254
6.987	-0.203	0.376	-0.372	0.269	-0.188	0.152	-6.413	0.253
7.491	-0.204	0.389	-0.382	0.279	-0.170	0.158	-7.446	0.258
8.033	-0.214	0.390	-0.392	0.283	-0.161	0.163	-8.110	0.258
8.613	-0.226	0.389	-0.404	0.284	-0.145	0.162	-9.126	0.254
9.236	-0.231	0.398	-0.417	0.292	-0.120	0.148	-10.516	0.253
9.903	-0.231	0.413	-0.418	0.311	-0.079	0.138	-12.047	0.263
10.618	-0.222	0.426	-0.411	0.337	-0.066	-0.189	-13.253	0.284
11.386	-0.217	0.439	-0.405	0.362	-0.038	-0.183	-14.043	0.307
12.208	-0.215	0.453	-0.405	0.380	-0.005	-0.087	-14.951	0.324
13.091	-0.212	0.470	-0.399	0.395	0.039	-0.022	-15.972	0.333
14.037	-0.213	0.486	-0.398	0.409	0.047	-0.003	-16.105	0.348
15.051	-0.219	0.499	-0.394	0.415	0.037	0.058	-15.290	0.362

Lanzano G., Felicetta C., Pacor F. - Metodology to identify reference rock sites - SIGMA2-XXXX-YY-ZZ

16.138	-0.225	0.510	-0.395	0.424	0.034	0.190	-14.602	0.375
17.305	-0.230	0.521	-0.403	0.440	-0.025	-0.188	-14.651	0.394
18.555	-0.237	0.532	-0.413	0.460	0.008	0.061	-14.963	0.414
19.896	-0.241	0.546	-0.425	0.479	0.011	0.036	-15.619	0.431
21.333	-0.234	0.553	-0.425	0.495	0.076	0.089	-17.544	0.437
22.875	-0.241	0.561	-0.433	0.509	0.131	0.365	-18.223	0.443
24.528	-0.242	0.566	-0.436	0.521	0.098	0.202	-18.178	0.460
26.300	-0.222	0.570	-0.415	0.537	0.090	-0.212	-19.666	0.465
28.201	-0.222	0.572	-0.417	0.550	0.167	-0.002	-21.082	0.471